



Contrasting appinites, vaugnerites and related granitoids from the NW Iberian Massif: insight into mantle and crustal sources

Gumer Galán¹, Gloria Gallastegui², Andrés Cuesta³, Guillermo Corretgé³, Ofelia Suárez³, and Luis González-Menéndez⁴

¹Departament de Geologia, Universitat Autònoma de Barcelona, Bellaterra, 08193, Barcelona, Spain

²Instituto Geológico y Minero de España (IGME, CSIC), Oviedo, 33005, Spain

³Departamento de Geología, Universidad de Oviedo, Oviedo, 33005, Spain

⁴Instituto Geológico y Minero de España (IGME, CSIC), León, 24006, Spain

Correspondence: Gumer Galán (gumer.galan@uab.cat) and Gloria Gallastegui (g.gallastegui@igme.es)

Received: 11 November 2022 – Revised: 20 August 2023 – Accepted: 23 August 2023 – Published: 18 October 2023

Abstract. Post-collisional Mg–K-rich mafic rocks with associated granitoids appear regularly in most orogens. They are relevant to evaluate the mantle role in the genesis of granitoids and thereby of the continental crust itself. The most characteristic Mg–K mafic rocks in the Variscan Iberian Massif are appinites and vaugnerites. Two examples with associated granitoids from NW Iberia have been compared to assess their mantle and crustal sources and the magmatic processes involved in their formation. Related granitoids are tonalites, granodiorites and monzonitic granites. Available whole-rock major and trace element compositions, as well as Sr and Nd isotopes, were used for this comparison, along with new Sr–Nd isotopic data. The appinite–granitoid association is calc-alkalic, whereas the vaugneritic one is calc-alkalic transitional to alkali-calcic. Vaugnerites are more enriched in Mg and K, compatible and incompatible trace elements and display more fractionated rare-earth element (REE) patterns than appinites. Associated granitoids provide similar differences. Appinites and vaugnerites have Sr and Nd crustal isotopic signatures resulting from partial melting of a different subduction-type metasomatised mantle: amphibole spinel lherzolites for appinites and more refractory and deeper amphibole phlogopite ± garnet peridotites for vaugnerites. Further interaction of these basic melts with coeval granitoids occurred during their ascent and emplacement. The monzonitic granites derived from partial melting of metaigneous acid granulites, without discarding contribution of metasediments and/or an increasing role of biotite incongruent melting in those related to vaugnerites. An assimilation with fractional crystallisation process between appinite magmas and granulites could explain tonalites and granodiorites. This process was not confirmed for granodiorites related to vaugnerites.

1 Introduction

High K calc-alkaline magmatism has been recognised in most post-collisional settings since the late Archean (Bonin, 2004; Fowler et al., 2008; Fowler and Rollinson, 2012; Guo et al., 2014; Xiong et al., 2015; Couzinié et al., 2016; Wang et al., 2019). This magmatism includes highly heterogeneous Mg–K mafic rocks, closely associated with post-collisional granitoids, which are particularly useful to understand the evolution of the lithosphere at the end of orogenic cycles.

Although subordinate to granitoids, the habitual occurrence of these Mg–K mafic rocks raises the issue of mantle contribution to the granitoid genesis, with mass and/or heat transfer, and therefore to the formation of new continental crust. In the outcrops of the Variscan orogen in western and central Europe, these mafic rocks receive different names: appinites, vaugnerites, redwitzites and durbachites, with compositions that are clearly distinct from those of usual igneous rocks (Sabatier, 1991). According to Sabatier (1991), they more closely resemble calc-alkaline lamprophyres, es-

pecially vaugnerites and durbachites, which display the highest Mg–K contents.

Following the Variscan collision (ca. 365–347 Ma) (Gutiérrez-Alonso et al., 2018, and references therein), different types of granitoids intruded into the most internal terranes of this orogen (Bonin, 2004), which extends through Europe and northern Africa (Díez Fernández et al., 2016, and references therein). In the NW of the Variscan Iberian Massif (Fig. 1a), the earliest granitoids were syntectonic calc–alkaline type (Corretgé et al., 2004; Cuesta and Galastegui, 2004) and deserve special attention because they are associated with ultramafic–mafic rocks of both appinite (Bailey and Maufe, 1916) and vaugnerite (Michel-Levy and Lacroix, 1887) types. More recently, appinites are described as “group of coeval plutonic and/or hypabyssal rocks ranging from ultramafic to felsic in composition, in which the hornblende is the dominant mafic mineral and typically occurs both as large prismatic phenocrysts and in the finer grained matrix” (Murphy, 2013). Vaugnerites are “a kind of micaeous diorite, which may be defined as coarse-grained, mesocratic igneous rock assemblages of biotite, amphibole and plagioclase, with interstitial quartz and potassium feldspar, and abundant accessory apatite, zircon, allanite and titanite” (Montel and Weisbrod, 1986; Sabatier, 1991). Although always subordinate to granitoids in the outcrops, the appearance of appinites and vaugnerites raises not only the general questions mentioned above, but also more specific ones on the nature of the mantle source(s) involved in their genesis, and the interaction processes with crustal components prior to and during their emplacement. Similarities and differences between Iberian appinites and vaugnerites were recently shown by Bea et al. (2021), using whole-rock major, trace element, and Sr and Nd isotopic compositions. They are interpreted as being derived from a mixture of one mantle and two crustal components. According to Bea et al. (2021), the mantle component could be the same for appinites and vaugnerites. One crustal component could have metasomatised the mantle prior to the generation of the mafic melts. The other crustal component could have been different and interacted diversely with the mafic appinitic and vaugneritic melts during their emplacement. Bea et al. (2021) also reached the conclusion that Iberian appinites and vaugnerites differ from typical arc rocks.

In this study, we will explore the similarities and differences between two Iberian plutonic complexes of appinites and vaugnerites, but we will also take into account the associated granitoids, allowing us to gain further insights into the nature of mantle and crustal sources and into the plausible interaction of the resulting magmas. To make the comparison, we will use previously published petrography, mineral major element compositions, and whole-rock major, trace element, Sr and Nd isotope compositions (Galán, 1987; Galán et al., 1996; Gallastegui, 2005), with new Sr–Nd isotopic data.

2 Geological setting and field relationships

2.1 The appinite–granitoid association

The appinite–granitoid association is included in the Vivero granitic massif (Galicia, NW Spain), which crops out at the core of the Lugo Dome (Capdevila, 1969), in the north-western part of the West Asturian–Leonese Zone (WALZ). It is limited to the west by a major shear zone (the Vivero fault) (Fig. 1a). This separates the WALZ from the Central Iberian Zone (CIZ), both terrains of the Iberian Massif (Fig. 1a). The general shape of the Vivero granitic massif is a laccolith (Galán, 1987; Marcos, 2013) formed by syntectonic meta- to peraluminous calc–alkaline granitoids and peraluminous leucogranites (Galán et al., 1996). The age of the country rocks is controversial: it has been argued that they are late Precambrian to early Cambrian metasediments (Martínez Catalán, 1985, and references therein) or that they are just early Cambrian metasediments (Marcos, 2013).

This study is only concerned with the calc–alkaline granitoids and associated ultramafic–mafic appinites (Galán, 1987). This association is located to the west of the Vivero massif (Fig. 1b). The granitoids crop out as a multi-intrusive layer of ca. 8 km long by 1–3 km wide, orientated N, NE–S following the direction of the Vivero fault. These granitoids are tonalites, granodiorites and porphyritic monzonitic granites. Sinuous contacts and concordant foliation between them suggest a coeval intrusion, cross-cutting earlier recumbent folds related to the first Variscan deformation episode (D1) conventionally established in the internal zones of the Variscan orogen (Marcos, 2013, and references therein). The ultramafic appinites appear mainly as decametric enclaves in peraluminous leucogranites (Fig. 1b). However, the mafic appinites also crop out as microgranular enclaves in tonalites and, as dykes, intruding into both the calc–alkaline granitoids and the country rocks. The ultramafic rocks, all hornblende bearing, are the most striking and common of the Vivero appinites. Their sinuous contact and decreasing grain size against the associated tonalites indicate their simultaneous injection (Galán, 1987). The intrusion of the whole association was facilitated by shear zones related to the major thrusting Variscan deformation episode (D2) dated at 320 Ma in the WALZ (Dallmeyer et al., 1997) or to the earliest movement of the Vivero fault. This structure was recently redefined as a crustal-scale extensional shear zone, postdating the D3 Variscan deformation episode but active at least between 303 ± 2 and 287 ± 3 Ma (López-Sánchez et al., 2015).

Five samples from Vivero (viz., a porphyritic monzonitic granite and four appinites) have been dated (Fernández-Suárez et al., 2000; López-Sánchez et al., 2015; Bea et al., 2021). Despite the field relationships suggesting coeval intrusion of the calc–alkaline granitoids and appinites, U–Pb geochronological results on zircons indicate older ages for the granitoids (323–314 Ma; Fernández-Suárez et al., 2000; López-Sánchez et al., 2015) than for the appinites (293–

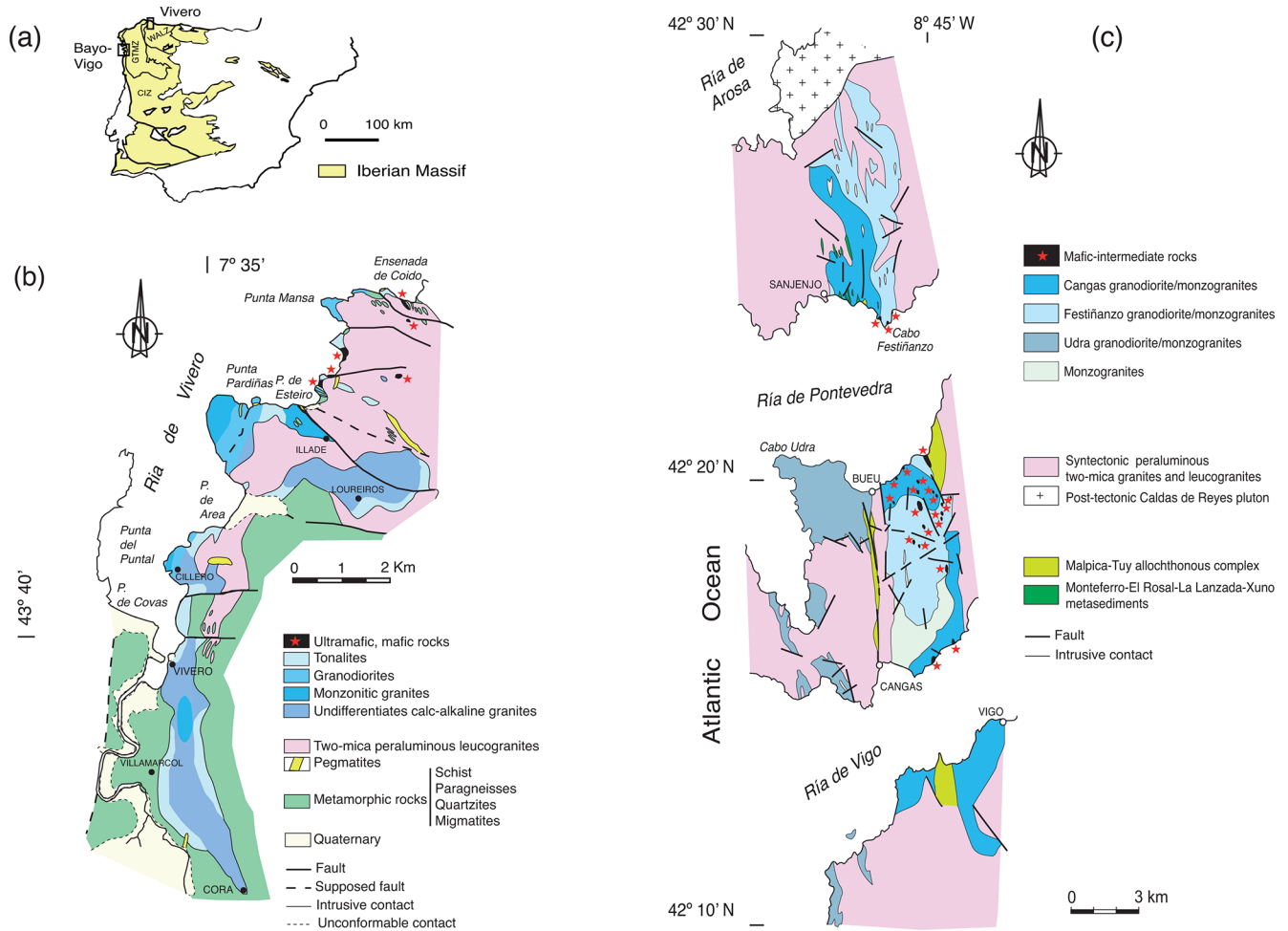


Figure 1. (a) Location of the two associations studied in the NW Iberian Massif: WALZ, CIZ and GTMZ stand for West Asturian–Leonese Zone, Central Iberian Zone and Galicia–Trás-os-Montes Zone respectively. (b) Geological map of the Vivero (ultramafic–mafic) appinite–granitoid association (modified after Galán et al., 1996). (c) Geological map of the southern part of the Bayo–Vigo (mafic-intermediate) vaugnerite–granitoid association (modified after Gallastegui, 2005).

289 Ma) (Fernández-Suárez et al., 2000; Bea et al., 2021). Therefore, only the age of the monzonitic granite agrees with field data interpretation. By contrast, the age of appinites is comparable to ages provided for the peraluminous two-mica leucogranites, the intrusion of which is considered simultaneous with the latest movement of the Vivero fault (297–287 Ma) (López-Sánchez et al., 2015). Three possible explanations are envisaged: (i) the age of the monzonitic granite is influenced by zircon inheritance, the presence of which is documented (Fernández-Suárez et al., 2000; López-Sánchez et al., 2015); (ii) the zircon U–Pb isotope system of the appinites was reset by the younger intrusion of peraluminous two-mica leucogranites (287 ± 3 Ma; López-Sánchez et al., 2015), which cross-cut and enclose both the appinites and related granitoids; and (iii) the area was affected by prolonged igneous activity, starting at 314 Ma with the intrusion of appinites and related granitoids and remaining at elevated temperatures until 287 Ma, when the massive intru-

sion of the peraluminous two-mica leucogranites took place. It then cooled slowly to below the zircon U–Pb closure temperature only after the cessation of igneous activity, as suggested for other Variscan areas (Klötzli et al., 2014, and references therein). The gap between 314 and 287 Ma may record the occurrence and duration of the thermal peak at the Lugo Dome, when all the rocks remained at elevated temperatures. Thus, the age of 287 Ma provided by appinites would reflect final cooling to temperatures below the closure temperature of U–Pb in Zircon. Taking into account that the age of 314 Ma was estimated avoiding inherited zircon cores in the monzonitic granite, either hypothesis (ii) or (iii) could explain the disagreement between the radiometric ages and field relationships. Hypothesis (iii) may require higher peak temperature than that recorded by host metamorphic rocks around the Vivero massif (620°C according to Reche et al., 1998). However, higher peak temperatures may have existed near the appinitic exposures, where migmatitisation of the host

metamorphic rocks is widespread. Whatever the reason and based on field relationships, we will assume the simultaneous intrusion of both Vivero appinites and syntectonic calc-alkaline granites at 314 Ma for the purpose of this study. We favour this age because it was determined on selected zones of five individual zircon grains in the monzonitic granite, which yielded concordant ages by laser ablation inductively coupled plasma mass spectrometry (LA-ICP-MS) (López-Sánchez et al., 2015). It is worth noting that a monazite fraction of the same granite, determined by isotope dilution thermal ionisation mass spectrometry (ID-TIMS) (Fernández-Suárez et al., 2000), also provided a concordant U–Pb age of 295 ± 2 Ma, suggesting that the U–Pb system in this mineral may have also been reset by later granitic intrusions.

2.2 The vaugnerite–granitoid association

The vaugnerite–granitoid association crops out in more internal zones of the Variscan basement, the Galicia–Trás-os-Montes Zone (GTMZ) (Farias et al., 1987), an allochthonous terrane that overthrusts the CIZ (Díez-Balda et al., 1990) (Fig. 1a). Vaugnerites and associated granitoids form the multi-intrusive Bayo–Vigo massif, of ca. 100 km long by < 10 km wide. This elongated intrusion, orientated N, NW–S, SE except in its northern section (N, NE–S, SW) (Fig. 1c), follows a dextral shear zone (the Malpica–Lamego line) (Llana Fúnez and Marcos, 2001), late to post-kinematic with respect to the Variscan deformation episode D3, dated at 310 ± 3 Ma (^{40}Ar – ^{39}Ar age; Gutiérrez-Alonso et al., 2015). However, Llana Fúnez and Marcos (2001) proposed that this fault reactivated a pre-existing crustal-scale thrust, which developed after the main Variscan collisional event (Díez Fernández et al., 2011). The geological setting is, therefore, similar to that of the Vivero appinite–granitoid association. The country rocks are metasediments and metaigneous rocks (Malpica–Tuy and Monteferro–Rosal–Lanzada–Xuno units) whose age is uncertain: Neoproterozoic to Silurian (Gallastegui, 2005, and references therein). The contacts between the Bayo–Vigo granitoids and these country rocks are intrusive and concordant with the main foliation (D2), although this foliation is locally cross-cut by granitoid veins.

The granitoids related to vaugnerites include three types of porphyritic granodiorites (viz., Cangas, Festiñazo, Udra) and monzonitic granites (Fig. 1c). Previous to Gallastegui (2005), nearby vaugnerites and related granitoids were studied by Gil Ibarguchi (1981) and Gil Ibarguchi et al. (1984). These authors proposed a lower crustal origin for the granitoids from pelites and greywackes or a mixture of both, the partial melting of which would have been triggered by the intrusion of mantle-derived vaugnerites at the lower crust. The granodiorites crop out as parallel bands and concordant with the internal foliation and main direction of the intrusion. The monzonitic granites are in diffuse contact with the Cangas granodiorite. Vaugnerites crop out at the eastern part of the massif as megaenclaves in the Cangas and Fes-

tiñazo granodiorites (Fig. 1c). They are very heterogeneous because of variable grain size (coarse- to fine-grained), mineral mode, and the distribution of felsic and mafic minerals. Bands and layers between vaugnerites and granodiorites with lobated, sinuous and diffuse contacts are common. Vaugnerites also appear as microgranular enclaves, either scattered in the granodiorites or as swarms hosted in monzonitic granites, with lobated, sinuous or diffuse contacts as well (Gallastegui et al., 1984). The enclave swarms form composite dykes or pods, up to 100 m long and 20 m wide, in contact with vaugnerites and the Cangas granodiorites. The orientation and internal foliation of the microgranular enclaves is concordant with that found in the granodiorites, monzonitic granites and vaugnerites, suggesting coeval intrusion of all of them (Gallastegui, 2005). This intrusion was most likely facilitated by D2 Variscan structures and took place before the development of the D3 shear zone. Vaugnerites and related granitoids are orientated with mylonitic microstructure in the most deformed outcrops. As in the Vivero association, the Bayo–Vigo vaugnerite–granitoid association was subsequently cross-cut by syntectonic peraluminous two-mica granites and leucogranites, and post-tectonic granodiorites (Fig. 1c).

Available U–Pb geochronological ages on zircons are contradictory. ID-TIMS determinations on discordant zircons from one vaugnerite and two granodiorites provided an upper intercept with the concordia at 350 ± 15 Ma (Gallastegui, 2005). Younger ages of 339.3 ± 1.2 and 337 ± 1 Ma were obtained by LA-ICP-MS for a vaugnerite and granodiorite respectively (Gutiérrez-Alonso et al., 2018). Nevertheless, other ID-TIMS determinations still provided the youngest ages of 322.8 ± 1.8 and 319.6 ± 0.7 Ma for vaugnerites (Rodríguez et al., 2007). These are close to a sensitive high-resolution ion microprobe (SHRIMP) age of 328 ± 2 Ma obtained for vaugnerites (Bea et al., 2021) and to chemical abrasion (CA)-ID-TIMS and SHRIMP ages of 326–315 Ma determined for the Bayo–Vigo porphyritic granodiorites (González-Menéndez et al., 2021). These younger ages would corroborate the theory of simultaneous intrusion of vaugnerites and granodiorites.

3 Methods

Mineral modes, mineral major element compositions, and whole-rock major, trace element, Sr and Nd isotope compositions were compiled from Galán (1987), Galán et al. (1996) and Gallastegui (2005). The new whole-rock Sr and Nd isotopic data were determined by ID-TIMS on seven vaugnerites and two monzonitic granites at the Geochronology and Geochemistry-SGIker facility of the Universidad del País Vasco UPV/EHU, using a Finnigan MAT262 mass spectrometer. Chemical procedures for Sr extraction are from Pin and Bassin (1992) and for Sm and Nd from Pin and Santos Zalduegui (1997). A $^{150}\text{Nd}/^{149}\text{Sm}$ mixed isotope

tracer was used. Blanks for Sm and Nd are negligible. Sr, Nd and Sm were loaded over Ta filaments and measured by Faraday in multicollection with corrections for mass fractionation by normalisation to $^{86}\text{Sr}/^{88}\text{Sr}=0.1194$ and $^{146}\text{Nd}/^{144}\text{Nd}=0.7219$ (Steiger and Jäger, 1977; Wasserburg et al., 1981). Analytical uncertainty was estimated to be $\pm 0.2\%$ on the $^{147}\text{Sm}/^{144}\text{Nd}$ ratio. The values and incertitude for individual measurements of $^{143}\text{Nd}/^{144}\text{Nd}$ and $^{87}\text{Sr}/^{86}\text{Sr}$ ratios for JNdi-1 and NBS-987 standards, under the same conditions, over different periods of analyses are the following: $^{143}\text{Nd}/^{144}\text{Nd}$ (JNdi-1) = 0.512097 ± 0.000001 (2σ ; $n=2$), $^{87}\text{Sr}/^{86}\text{Sr}$ (NBS-987) = 0.710261 ± 0.000017 (2σ ; $n=2$). The values obtained for the standards are comparable to those published by most laboratories worldwide. They lie within the certified range for the values obtained in the validation test of the JNdi-1 (Tanaka et al., 2000) and for the NBS-987 (Wise and Waters, 2007).

4 Petrography

4.1 Appinites and related granitoids

The Vivero appinite suite includes *ultramafic rocks*. Their petrographic names, main microstructures, essential, accessory and secondary minerals are included in Table 1 (see also Fig. 2a for their modal classification). There are fine-grained peridotites and pyroxenites (grain size < 1 mm) and coarse-grained hornblendites (grain size up to 5 cm). Cumulate microstructures are characteristic. Cumulus minerals are olivine, clinopyroxene and orthopyroxene. The main intercumulus minerals are amphibole and, less frequently, phlogopite (Fig. 3a). Olivine is only present in ultramafic appinites forming embayed and skeletal crystals. Orthopyroxene (up to 10 vol %) is subordinate to clinopyroxene (1 vol %–50 vol %). Orthopyroxene appears as anhedral, often poikilitic, crystals including olivine and clinopyroxene. Clinopyroxene forms anhedral crystals partially or completely replaced by amphibole. Amphibole appears as (i) large subhedral poikilitic crystals (Amp 1), with brown cores that give way to fibrous colourless rims through green zones; inclusions are mainly of anhydrous mafic silicates (Fig. 3a); (ii) interstitial fibrous colourless crystals (Amp 2) (Fig. 3b); and (iii) colourless crystals, pseudomorphosing clinopyroxene (Amp 3) (Fig. 3a). Phlogopite is seen intergrown with Amp 1 or forms isolated poikilitic crystals (Fig. 3c).

In mafic *appinites* (Table 1; Fig. 2b) (M (mafic minerals) > 40 vol % or 50 vol %) amphibole mode, although variable, is typically higher than biotite mode (amphibole / biotite ratio ranges from 0.5 to 84). Olivine and orthopyroxene are absent although some clinopyroxene crystals remain. Grain size varies from coarse (up to 5 cm in pegmatoid varieties) to fine grained (1 mm). Coarse-grained rocks show cumulate microstructure with amphibole as the main cumulus

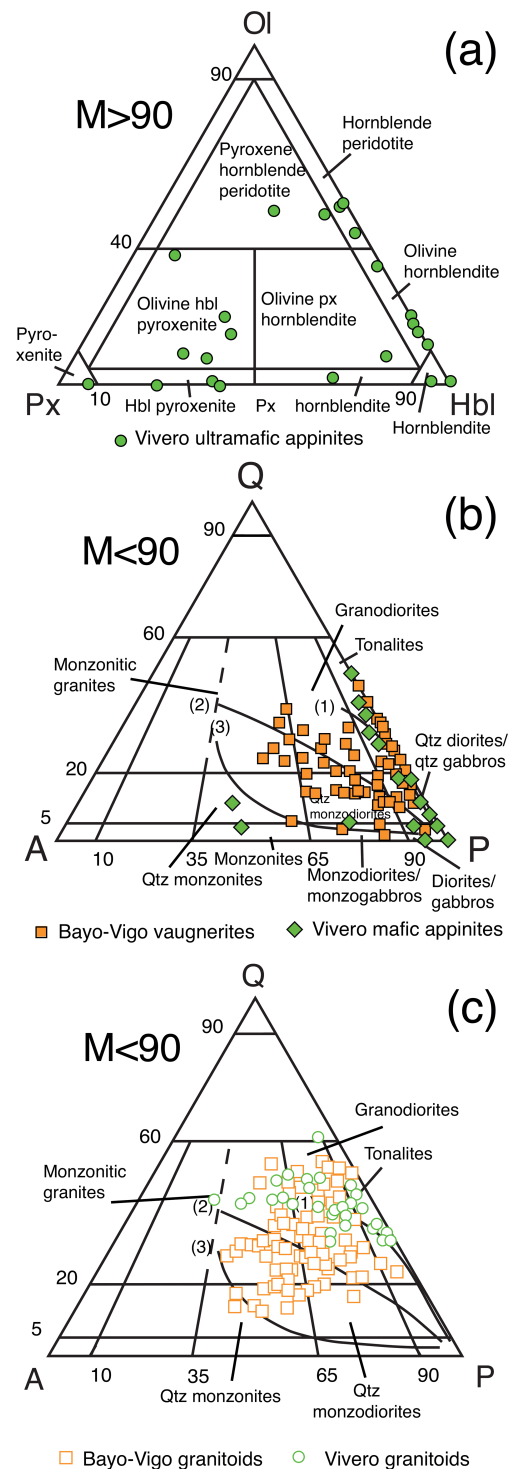


Figure 2. (a) Olivine–pyroxene–hornblende diagram with the nomenclature for Vivero ultramafic appinites. (b) Q–A–P diagram with the modal classification of mafic appinites from Vivero and of vaugnerites from Bayo–Vigo; (1), (2) and (3) lines refer to trondhjemite, granodioritic and monzonitic calc–alkaline plutonic series (Lameyre and Bowden, 1982). (c) Q–A–P diagram with the modal classification of granitic rocks from Vivero and Bayo–Vigo; (1), (2) and (3) as before. Modal triangular diagrams after Le Maitre (2002).

Table 1. Main types of rocks, microstructures and mineralogy of the two studied associations.

Main rock types	Vivero appinitic association					Bayo-Vigo vaugneritic association				
	Petrographic names	Micro structures	Essential minerals	Accessory minerals	Secondary minerals	Petrographic names	Micro structures	Essential minerals	Accessory minerals	Secondary minerals
Ultramafic	± Px–Amp peridotites ± Px–Ol hornblendites Hornblendites ± Ol–Amp pyroxenites Pyroxenites	Cumulates mainly poikilitic	Ol, Cpx, Opx, Amp, Pl	Ap, Chr, Mag, Ilm sulfides	Srp, Mag, Ch, Tlc, Chl	–	–	–	–	–
Mafic	Bt–Amp diorites, Qtz diorites, tonalites, monzonites, Qtz monzonites	Cumulates, subhedral granular	Amp, Bt, ± Cpx, Pl, ± Mc, ± Qtz	Ilm > Tm, Ap, Zm, Aln, Ep, Sulfides	Ser, Saussurite, Chl, Tn, Ep	Amp–Bt gabbros, gabbro–diorites, monzogabbro–diorites, Qtz gabbro–diorites, Qtz monzogabbro–diorites, monzodiorites, monzonites, tonalites, granodiorites, melagranites Bt tonalites, granodiorites, monzonitic granites	Subhedral granular, ophitic–poikilophitic varieties	Cpx > Opx, Amp, Bt, Pl, Kfs, Qtz	Chr, Ilm, Tm, Ap, Zm, Aln, Ep, Sulfides	Ser, Saussurite, Chl
Granitoids	Amp–Bt tonalites, Bt tonalites, granodiorites ± Ms–Bi monzonitic granites	Subhedral–anhedral granular protomylonitic to mylonitic porphyritic in granodiorites and monzonitic granites	Bt, Amp, ± Cpx, Pl, Kfs, Qtz, ± Ms	Tm > Ilm, Ep, Zm, Ap, Grt, Sulfides	Ser, Chl, Tn, Ep	Bt granodiorites (Festizanzo, Udra, Cangas), Ms–Bt monzonitic granites	Porphyritic, anhedral granular	Bt, Pl, Kfs, Qtz	Ms, Zm, Ap, Aln, ± Tur, Ilm, Rt, ± Ft	Ser, Chl

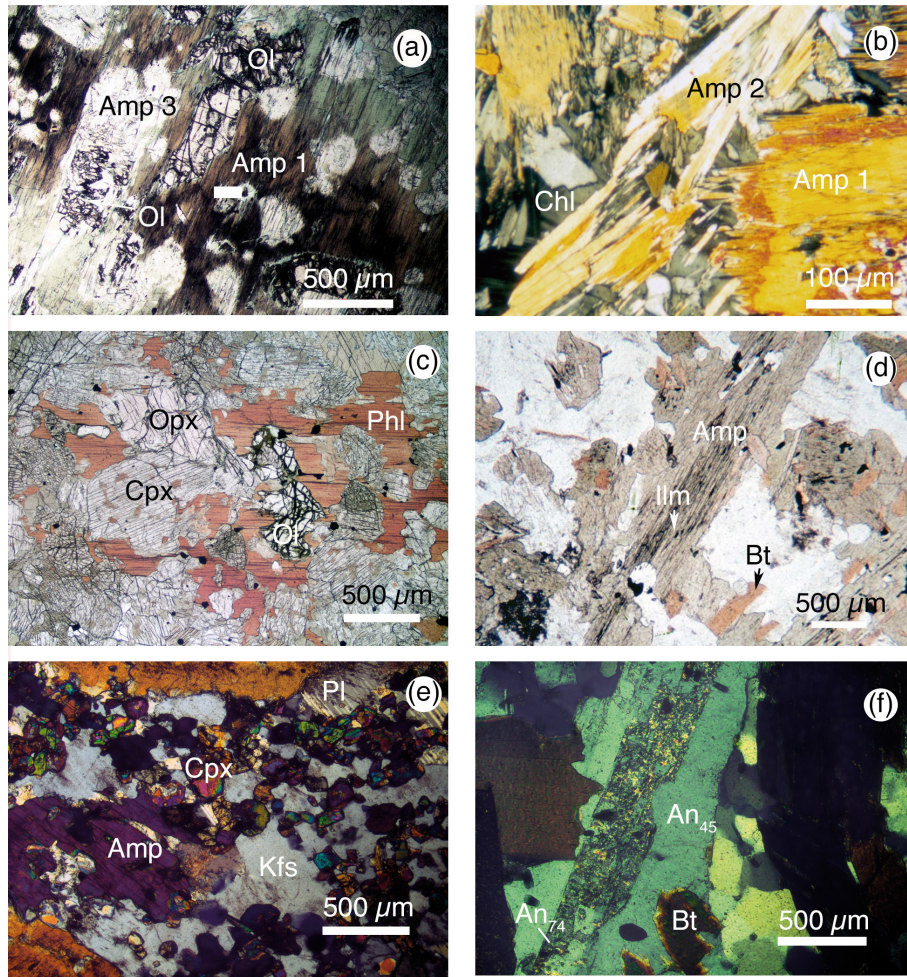


Figure 3. Microstructures of Vivero ultramafic and mafic appinites. **(a)** Large amphibole poikilitic crystal (Amp 1), with brown core with tiny ilmenite inclusions and/or exsolutions in black, passing to green zones in hornblendites; other inclusions are of olivine and pseudomorphs formed of white amphibole crystals (Amp 3). **(b)** Zoned Amp-1 crystal with fibrous rim, interstitial fibrous amphibole crystals (Amp 2) and chlorite in hornblendites. **(c)** Phlogopite crystal including olivine, clinopyroxene and orthopyroxene in ultramafic appinites. **(d)** Relationships between amphibole, ilmenite and biotite crystals in mafic appinites. **(e)** Clinopyroxene and amphibole cumulus crystals surrounded by intercumulus plagioclase and K feldspar in an appinite (monzonite type) **(f)** Plagioclase crystal with a resorbed or skeletal calcic core partially altered to sericite and surrounded by a more albitic rim in an appinite (quartz diorite). Mineral abbreviations after Whitney and Evans (2010).

phase. Medium- to fine-grained rocks show subhedral granular microstructure. Amphibole shows brownish cores with tiny ilmenite inclusions (Fig. 3d). In the coarsest grained rocks, amphibole forms long hollow prismatic crystals (up to 7 cm). Felsic minerals fill the holes, a typical feature of crystallisation under high P_{H_2O} conditions (Wells and Bishop, 1955; Key, 1997). Biotite is closely associated with amphibole, either as inclusions or pseudomorphosing this mineral. Microcline is only present in rare monzonites (Fig. 2b) as large interstitial crystals enclosing mafic minerals (Fig. 3e). Plagioclase (An_{74-45}) forms subhedral crystals, with normal discontinuous (Fig. 3f), oscillatory and patchy zoning. Most mafic appinites follow the trondhjemitic (1) trend of the calc-alkaline plutonic series (Lameyre and Bowden,

1982) (Fig. 2b). Only three samples, with high modal K feldspar (the monzodiorite, monzonite and quartz monzonite in Fig. 2b), roughly follow the monzonitic (3) trend.

The nomenclature and the main mineralogical and petrographic features of *granitic rocks* associated with appinites are also shown in Table 1, and their modal classification is in Fig. 2c. In Vivero, amphibole biotite tonalites outnumber the other granitic rocks. These tonalites differ from mafic appinites, which are locally included as microgranular enclaves, by lower M index (< 35) and amphibole / biotite ratio (2–0). They are medium-grained subhedral–anhedral granular rocks, with crystal orientation. They show clots of light-green amphibole at the core with tiny quartz inclusions, which give way to greener crystals and biotite at the rim.

These clots occasionally enclose relic clinopyroxene. Plagioclase (An_{64-32}) is present as subhedral crystals with complex zoning. K feldspar forms anhedral crystals, with a few perthites and local microcline twinning. Myrmekites are frequent at the contact between K feldspar and plagioclase. Quartz ocelli or xenocrysts, with amphibole–biotite rims, are occasionally observed. Biotite tonalites and granodiorites are fine- to medium-grained subhedral–anhedral granular rocks. They are orientated and with protomylonitic microstructure in the most deformed outcrops. They also differ from amphibole biotite tonalites due to the presence of scarce K-feldspar megacrysts, less calcic plagioclase (An_{45-27}) and accessory garnet. Finally, porphyritic muscovite biotite monzonitic granites are coarser-grained rocks, with K-feldspar megacrysts (2–3 cm) in an anhedral granular matrix. Protomylonitic to mylonitic microstructures are also frequent. Their plagioclase (An_{37-28}) is less calcic than that of the granodiorites. The Vivero granitoids plot between the calc-alkaline plutonic series (1) and (2) of Lameyre and Bowden (1982) (Fig. 2c).

4.2 Vaugnerites and related granitoids

The Bayo–Vigo *vaugnerites* were distinguished into two groups (Table 1). One group, mainly megaenclaves, is mostly melanocratic with few leucogabbros. Its amphibole / biotite ratio ranges from 0.1 to 2.8, but it is usually < 1. Clinopyroxene (up to 13 vol %) and rare orthopyroxene are present. The second group of *vaugnerites*, interlayered with coeval granitoids and as microgranular enclaves, is mainly biotitic and melanocratic. Grain size and microstructures of *vaugnerites* are similar to those of mafic appinites, except for the coarsest-grained rocks (gabbros), which show poikilophitic microstructures: mafic minerals, biotite in particular, also include plagioclase crystals (Fig. 4a–b). Pyroxenes are commonly surrounded by amphibole. The most characteristic biotite crystals are large (up to 5 cm) and tabular shaped, including relic clinopyroxene rimmed by amphibole, and plagioclase (Fig. 4a). In the gabbros, amphibole forms large, brown-green crystals (similar to Amp 1 in ultramafic appinites) with clinopyroxene and plagioclase inclusions (Fig. 4b). There are also fibrous colourless crystals (similar to Amp 2) and others in pseudomorphs or clots (similar to Amp 3). The amphibole clots (Fig. 4c) show colourless cores, which become greener towards the border and can enclose small quartz inclusions, clinopyroxene relics, biotite and opaque (Cr-rich spinel) \pm titanite crystals. Plagioclase crystals (An_{80-17}) can be isolated or grouped as glomerocrysts and display complex zoning. The most calcic compositions correspond to corroded or skeletal cores (Fig. 4d) and to rims enveloping less calcic poikilitic cores, all in turn mantled by more albitic compositions (Fig. 4e). The inclusions are biotite, amphibole, quartz, opaques, apatite and even plagioclase. Potassium feldspar is present as interstitial anhedral crystals, at times poikilitic, and can replace plagioclase.

Quartz crystals are mostly interstitial and anhedral but also appear as millimetric to centimetric quartz \pm feldspar ocelli, surrounded by amphibole \pm biotite \pm titanite (Fig. 4f). The three evolutionary trends of the calc-alkaline plutonic series (Fig. 2c), trondhjemite (1), granodioritic (2) and monzonitic (3) are observed among the *vaugnerites*. This data scattering is common among *vaugnerites*, which is in part due to their high mafic mineral mode, particularly biotite mode. In addition, the mingling between *vaugnerites* and associated granitoids (Gallastegui, 2005) can contribute to this data dispersion.

In contrast to the appinitic suite, biotite porphyritic granodiorites are more frequently found (Fig. 2c) among *granitoids* related to *vaugnerites*. The three granodiorite types (Table 1) are coarse-grained and texturally similar to the porphyritic biotite monzonitic granites of Vivero. However, they differ in the abundance and size of the K-feldspar megacrysts, which increases from the Cangas (1–2 cm at the long axis) to the Udra type (4–12 cm). They also vary in showing decreasing An content in plagioclase crystals, which usually show complex zoning (46 %–20 % in the Cangas type, 36 %–20 % in the Festiñanzo type and 31 %–17 % in the Udra type). Potassium-feldspar megacrysts usually display microcline twinning, perthites and myrmekites at the contact with plagioclase. Replacement of plagioclase by K feldspar is common in the matrix. Biotite (23 vol %–5 vol %) in the granodiorites appears either as clusters (Festiñanzo and Cangas granodiorites), where the crystals show decussate orientation, or as isolated crystals (Udra granodiorites). It is usually associated with accessory minerals, including muscovite, whose mode increases in the Udra granodiorite (up to 2.6 vol %). As regards the \pm muscovite biotite monzonitic granites, they are coarse- to medium-grained rocks, mostly equigranular and anhedral, and more leucocratic than the granodiorites. An range in plagioclase is similar to that of the Cangas granodiorite, but this component increases when these monzonitic granites enclose swarms of microgranular enclaves. Similar to *vaugnerites*, related granitoids plot between trondhjemite (1) and monzonitic (3) series (Fig. 2c). The great dispersion is in part explained by the effect of K-feldspar megacrysts on the counting-point method used for modal analyses (Gallastegui, 2005).

5 Mineral chemistry

Major element compositions of mafic minerals present in the two associations, along with those of olivine only observed in ultramafic appinites, will be used to highlight similarities and differences (see Fig. 5) and to ascertain their origin.

Olivine in ultramafic appinites shows forsterite (Fo) content or magnesium number ($Mg\# = Mg/(Mg + Fe_T + Mn)$), in atoms per formula unit (apfu) from 82 to 68, decreasing from peridotites to hornblendites.

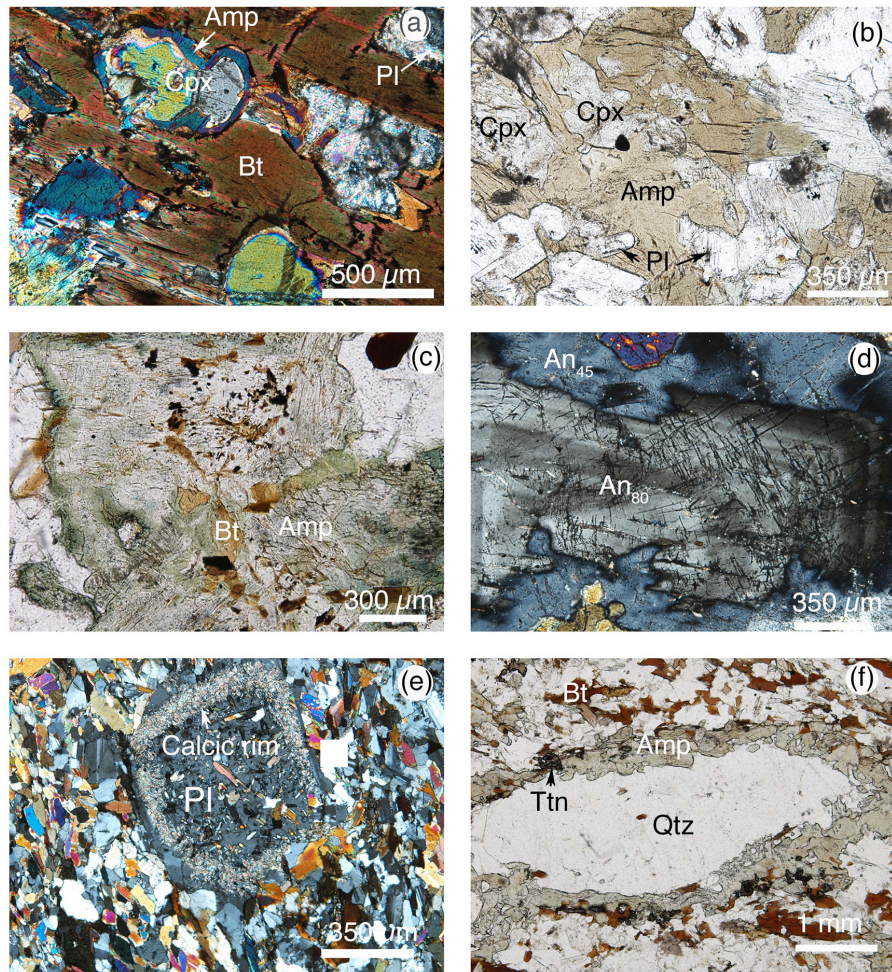


Figure 4. Microstructures of the Bayo–Vigo vaugnerites. (a) Clinopyroxene rimmed by amphibole, amphibole and saussuritized plagioclase crystals in poikilitic biotite. (b) Clinopyroxene and plagioclase within brownish-green amphibole. (c) Amphibole clot surrounding relic clinopyroxene with corroded biotite inclusions. (d) Resorbed or skeletal calcic plagioclase core surrounded by a more albitic rim. (e) Poikilitic plagioclase core rimmed by a saussuritized calcic zone in turn mantled by more albitic compositions. (f) Quartz ocelli surrounded by amphibole, biotite and titanite.

Orthopyroxene in the ultramafic appinites is enstatite or aluminian enstatite ($Wo_{0.7-2.5} En_{74-80} Fs_{17-25}$), with Mg# ranging from 81 to 75. It shows lower amounts of Al_2O_3 (< 3.0 wt %), TiO_2 (< 0.20 wt %) and Cr_2O_3 (< 0.19 wt %) than orthopyroxene from mantle fertile lherzolites (e.g. Galán et al., 2011), from which it also differs in having lower Mg#. By contrast, the rare orthopyroxene in vaugnerites is enstatite or ferrian enstatite ($Wo_{1.5-3.8} En_{56-61} Fs_{35-41}$), with lower Mg# (61–58) and Al_2O_3 concentration (0.59 wt %–1.92 wt %) than in ultramafic appinites.

Clinopyroxene is diopside and augite close to diopside ($Wo_{45-50} En_{44-50} Fs_{4.2-10}$) in ultramafic appinites. A few analyses can be qualified as chromian and occasionally aluminian–chromian. Mg# (94–84) is significantly higher than in orthopyroxene and olivine. TiO_2 , Al_2O_3 and Cr_2O_3 are below 0.23 wt %, 2.79 wt % and 0.86 wt %, respectively.

The concentration of these three components is also lower than in typical mantle lherzolite clinopyroxene (e.g. Galán et al., 2011), but their Mg#'s overlap. It is worth noting that clinopyroxene in tonalites of the granitoid sequence, corresponding to a relic crystal in an amphibole clot, shows similar composition to clinopyroxene in ultramafic appinites, which suggests it is a xenocryst. Clinopyroxene in vaugnerites is also diopside or augite close to diopside ($Wo_{39-50} En_{32-43} Fs_{11-24}$), with a few analyses classified as aluminian or aluminian–chromian. It mainly differs from that found in appinites in that it has lower Mg# (79–58). Ti vs. Ca + Na for clinopyroxene of basic and intermediate rocks formed at 0.4–1.0 GPa pressure (Fig. 5a; Leterrier et al., 1982; Molina et al., 2009), the most likely conditions for the intrusion of appinites and vaugnerites, does not allow the discrimination of the origin of this mineral, either from alkaline or

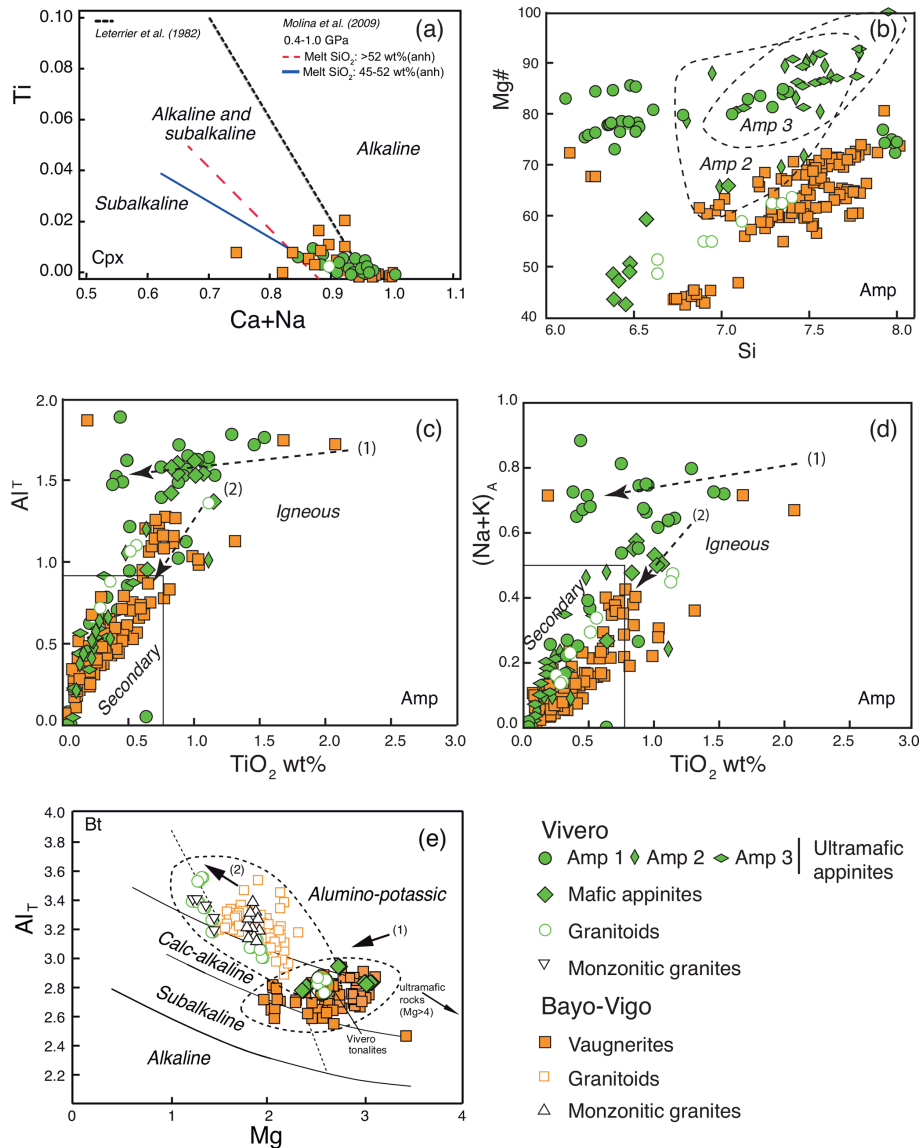


Figure 5. (a) Ti vs. Ca + Na, in atoms per formula unit (apfu), for discriminating between clinopyroxene-saturated alkaline and subalkaline basalts at 1 bar (Leterrier et al., 1982) and equivalent boundaries for anhydrous basic and intermediate melts at 0.4–1.0 Gpa (Molina et al., 2009). (b) Mg# vs. Si (in apfu) showing the different types of amphiboles in the appinites, vaugnerites and related granitoids. (c) Al in the tetrahedral site (Al^T) vs. TiO_2 concentrations for amphiboles. (d) Na + K in the A site vs. TiO_2 concentration in amphiboles. The (1) and (2) in (b) and (c) are comparable to trends defined by primary amphiboles and by both primary and secondary amphiboles, respectively, in other Iberian appinites (Molina et al., 2009; Cambeses et al., 2021). (e) Total Al (Al_T) vs. Mg (all in apfu) (Nachit et al., 1985) for biotites of the different rock types (phlogopites of ultramafic appinites are not represented). Trend 1 is for biotites of mafic appinites and vaugnerites, while trend 2 is for biotites from related granitoids.

subalkaline magma type: clinopyroxene from both appinites and vaugnerites straddles both fields, and most analyses plot within the field shared by clinopyroxene in equilibrium with alkaline or subalkaline melts (Molina et al., 2009). Nevertheless, the fact that clinopyroxene and orthopyroxene co-exist, especially in the ultramafic appinites, points to SiO_2 -saturated melts more akin to subalkaline types.

Amphiboles from the two associations display similarities and differences (Fig. 5b–d). Large amphibole crystals

(Amp 1) in the ultramafic appinites are pargasite at the brown cores and tremolite, actinolite, and cummingtonite at the colourless rims (Fig. 3a–b), passing through green zones of magnesio ferri hornblende and magnesio hornblende (Hawthorne et al., 2012). Mg# ranges from 64 to 86 (Fig. 5b) and can increase from the core towards the rim of a single crystal. TiO_2 reaches up to 1.5 wt % (Fig. 5c–d). Most Amp-1 type compositions show a slight decrease in Al at the T site (Al^T) and Na and K at the A site [$(Na + K)_A$], with

decreasing TiO₂ (trend 1; Fig. 5c–d). Compositions of interstitial amphibole (Amp 2) are tremolite, magnesio hornblende and, more rarely, cummingtonite, with the Mg# range (92–79) overlapping values of the Amp-1 rims (Fig. 5b). Maximum TiO₂ (0.64 wt %) concentration is lower than in Amp 1 (Fig. 5c–d). Amphibole in pseudomorphs (Amp 3; Fig. 5a) is tremolite–actinolite, also with Mg# from 93 to 78 and low TiO₂ (up to 0.33 wt %). In mafic appinites, amphibole is also pargasite or magnesio hornblende but with much lower Mg# (66–43) than in the ultramafic ones. TiO₂ is below 1.1 wt %. Finally, amphibole is magnesio hornblende or magnesio ferri hornblende in the tonalites of the granitoid sequence, with similar Mg# (63–49) and TiO₂ concentrations (up to 1.1 wt %) to amphibole in mafic appinites. All these amphiboles are characterised by a stronger decrease of Al^T and [(Na + K)_A] with TiO₂ (Trend 2; Fig. 5c–d) than in ultramafic appinites. Trend (1) and (2) in Fig. 5c–d are comparable to those defined by primary (1) and by both primary and secondary amphiboles (2), in other Iberian appinites (Molina et al., 2009; Cambeses et al., 2021). In vaugnerites, most analyses correspond to amphiboles in clots, which are actinolite grading to magnesio hornblende or magnesio ferri hornblende from colourless cores towards the greener rims (Fig. 4c). These amphiboles have less Al^T, [(Na + K)_A] and higher Mg# (81–43), for similar TiO₂ concentration, than amphiboles from mafic appinites, being more similar to amphiboles from tonalites of the Vivero granitoid sequence (Fig. 5b–d). Compositions of pargasite or magnesio hastingsite, equivalent to those of brown cores in ultramafic appinites (Amp 1), were only found in vaugneritic gabbros (Fig. 4b), but those from vaugnerites show lower Mg# (81–43) and slightly higher TiO₂ values (< 2.2 wt %). Nevertheless, this difference is not general, because primary Amp 1 in other Iberian appinites shows higher TiO₂ contents (up to 5 wt %) (Molina et al., 2009) than in the appinites and vaugnerites of this study. However, it should be borne in mind that TiO₂ in Amp 1 from Vivero ultramafic appinites could have been influenced by the co-existence of ilmenite (Fig. 3a).

Phlogopite compositions were analysed in ultramafic appinites. Mg# ranges from 89 to 77. Al₂O₃ concentration varies from 14.7 wt % to 17.1 wt %, and TiO₂ can reach up to 2.0 wt %. These compositions show lower Mg# than typical mantle phlogopites and are characteristic of ultramafic cumulates (McDonough and Rudnick, 1998). *Biotite* compositions in mafic appinites and vaugnerites have Mg# < 89 and provide a positive correlation in the total Al (Al_T; apfu) vs. Mg diagram (Nachit et al., 1985; trend 1 in Fig. 5e). By contrast, Mg and Al_T show a negative correlation in granitoid biotites (trend 2 in Fig. 5e), although those related to vaugnerites plot more scattered and show higher Mg values for similar Al_T values. Monzonitic granites from the two associations are highlighted with different symbols in Fig. 5e, because those related to vaugnerites follow a distinct evolution trend, with variable Al_T at constant Mg. Interestingly, these gran-

ites include swarms of vaugneritic microgranular enclaves (Gallastegui, 2005, and references therein). Figure 5e also illustrates that biotites from mafic appinites and from related hornblende–biotite tonalites of the granitoid sequence compare well with vaugnerite biotites, except that TiO₂ contents are higher in vaugnerites (up to 4.3 wt %) than in appinites (up to 3.0 wt %).

6 Whole-rock geochemistry

6.1 Major and minor elements

The ultramafic appinites from Vivero are mostly basic rocks with total alkalis < 2 wt % (Fig. 6a) and aluminium saturation index (ASI) < 1.09 (Frost et al., 2001). The mafic appinites are basic to intermediate with ASI < 1.08. The SiO₂ range of vaugnerites varies from basic to acid. Most of them are metaluminous (0.6 < ASI < 1.2), except for those forming microgranular enclaves, which are the most peraluminous and acid. In the granitoids related to appinites, SiO₂ concentration increases from tonalites towards monzonitic granites (Fig. 6a–d), and their ASI ranges from 0.9 in tonalites to 1.5 in one granodiorite. The Bayo–Vigo granodiorites and monzonitic granites exceed SiO₂ concentration of most acid vaugnerites and are peraluminous (1.0 < ASI < 1.2).

In the total alkalis vs. SiO₂ diagram (TAS) (Le Maitre, 2002), most rocks of the appinite–granitoid association are subalkaline, whereas most rocks of the vaugnerite–granitoid association straddle the limit between the subalkaline and alkaline series (Fig. 6a). Both associations are magnesian (Fig. 6b), although this is more accentuated in the vaugnerite one, calc–alkalic in Vivero, and range from calc–alkalic to alkali–calcic in Bayo–Vigo (Fig. 6c) (Frost et al., 2001).

The K₂O vs. SiO₂ diagram (Le Maitre, 2002; Fig. 6d) illustrates that, although the two associations largely overlap with respect to K₂O concentrations, the highest K₂O abundances correspond to the vaugneritic type. Thus, the appinite–granitoid association is mainly a high-K calc–alkaline series, whereas the vaugnerite–granitoid association straddles the limits from medium-K calc–alkaline series to shoshonite series. However, the similarity between shoshonitic and vaugneritic series in this diagram is only apparent (Scarrow et al., 2009a; Bea et al., 2021). According to these authors, vaugnerites differ from shoshonites in being more magnesian, richer in light ion lithophile and high field strength elements (LILEs and HFSEs, respectively) and in having higher light rare-earth / heavy-rare earth ratios than the latter. Another difference is that Sr and Nd isotopic compositions of vaugnerites are crust or lithospheric mantle-like, whereas shoshonites have depleted, asthenospheric mantle isotope signature.

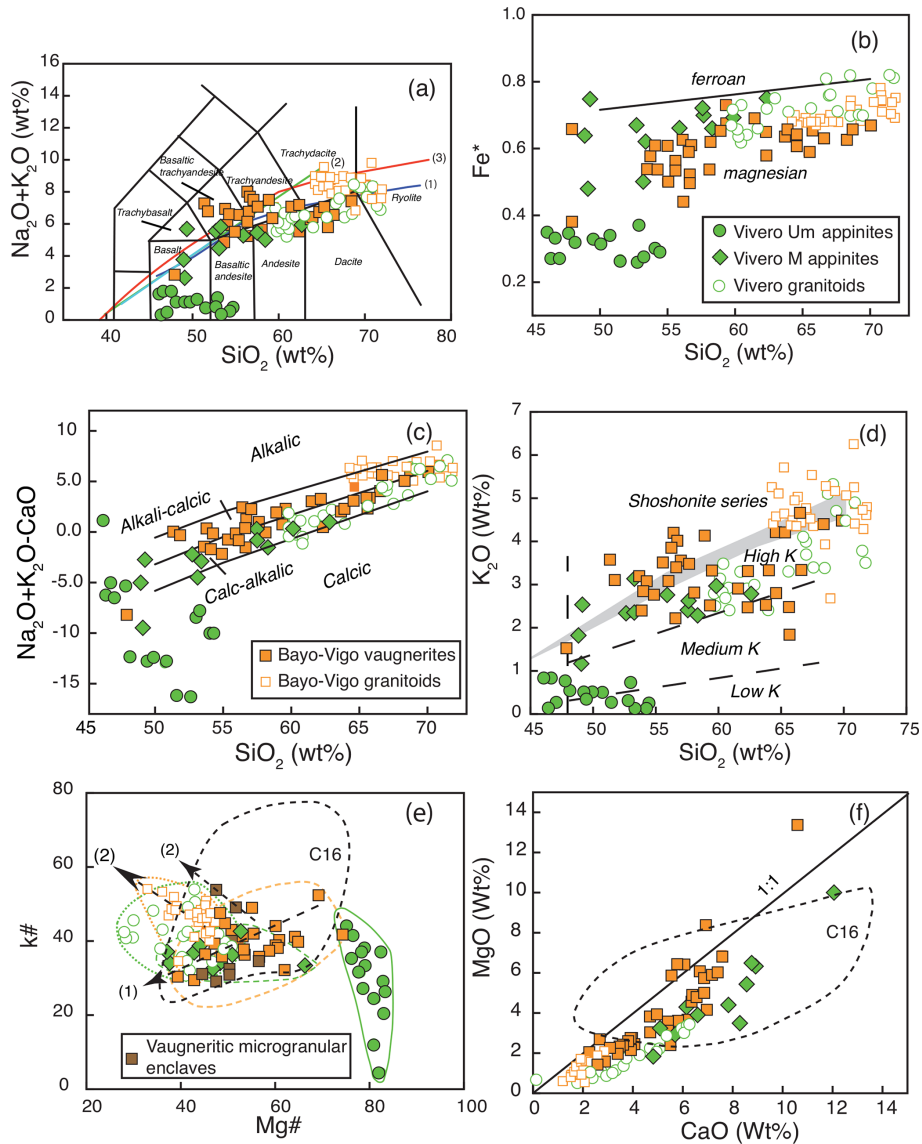


Figure 6. (a) Total alkalis vs. SiO_2 (TAS) diagram indicating the equivalent volcanic rocks of the two associations. Boundaries between alkaline and subalkaline series of Kuno (1966), MacDonald (1968), and Irvine and Baragar (1971) are also illustrated. (b) Fe number ($\text{Fe}^* = \text{FeO}_T / (\text{FeO}_T + \text{MgO})$) vs. SiO_2 , oxides in wt %, with the boundary between ferroan and magnesian plutons (Frost et al., 2001). (c) Modified alkali–lime index (MALI) (Frost et al., 2001) vs. SiO_2 with the boundaries between alkalic, alkali–calcic, calc–alkali and calcic series. (d) K_2O vs. SiO_2 diagram with the subdivision for subalkaline rocks of Le Maitre (2002) (dashed lines). The band between shoshonite series and high K series is from Rickwood (1989). (e) $\text{K}\#$ vs. $\text{Mg}\#$ for Vivero appinites and Bayo–Vigo vaugnerites, contrasting the evolving trends. Excluding the ultramafic rocks, $\text{K}\#$ remains almost constant for variable $\text{Mg}\#$ in mafic appinites, whereas in the related granitoids $\text{K}\#$ displays scattered. By contrast, $\text{K}\#$ and $\text{Mg}\#$ show a positive correlation in vaugnerites (trend 1) and a negative one in related granitoids and some of the vaugneritic microgranular enclaves (trends 2). The Bayo–Vigo vaugnerites are less potassic than those from the Massif Central, France (C16; Couzinié et al., 2016). (f) MgO vs. CaO diagram showing that the studied associations are more calcic than magnesian, excepting ultramafic appinites (not represented) and a few vaugnerites; vaugnerites are closer to the 1 : 1 ratio than appinites, and both mafic appinites and vaugnerites plot within the field of post-collisional Variscan mafic magmatism from the eastern Massif Central (C16; data from Couzinié et al., 2016).

The diagram of K number ($K\# = 100 \cdot K_2O / (K_2O + Na_2O)$) vs. Mg# ($Mg\# = 100 \cdot MgO / (MgO + FeO_T)$) (all oxides in moles) (Fig. 6e) serves to illustrate different evolving trends of the two associations. Excluding the ultramafic appinites, which plot apart from the general trend due to their cumulus character, the mafic appinites show nearly constant K# with decreasing Mg#, whereas in the related granitoids K# displays scattered with no clear trend. By contrast, most vaugnerites are characterised by simultaneous decreasing of both K# and Mg# (trend 1; Fig. 6e), whereas in the related granitoids and several vaugnerite microgranular enclaves, K# increases when Mg# decreases (trend 2; Fig. 6e). Trend (1), defined by decreasing alkalis, especially K_2O , with the differentiation of most vaugnerites (see also Fig. 6a, d) is typical of the vaugnerites from the Massif Central of France (MCF) (Sabatier, 1991), representing the most typical Variscan post-collisional mafic magmatism of this area (Couzinié et al., 2016). However, MCF vaugnerites can be more potassic than those from Bayo–Vigo (Fig. 6e), which would be classified between redwitzites and vaugnerites, as previously observed by Errandonea-Martín et al. (2018). Also, trend (1) in Fig. 6e could be correlated with the trondhjemite calc–alkaline plutonic trend defined by the Bayo–Vigo vaugnerites (Fig. 2b): biotite and amphibole modes might decrease with magmatic differentiation, causing lower Mg#, whereas quartz increases at constant K feldspar and decreasing plagioclase reducing K#. By contrast, trend (2) in Fig. 6e could reflect decreasing biotite, amphibole at decreasing plagioclase, and increasing quartz and K feldspar and thus be correlated with the granodioritic calc–alkaline plutonic trend of vaugnerites in Fig. 2b.

The two studied associations can be also differentiated by using the MgO vs. CaO diagram (Sabatier, 1984; Fig. 6f), where the ultramafic appinites (not represented) show $MgO > CaO$ abundance and a negative correlation between the two components. This is mainly due to olivine fractionation. By contrast, the other appinites and related granitoids display $MgO < CaO$, just as most vaugnerites and related granitoids do. However, the vaugnerites can show $MgO > CaO$, which is the case of similar rocks in the MCF (data from Couzinié et al., 2016).

Regarding minor components, the two associations show similar TiO_2 contents in mafic rocks and related granitoids (Supplement, Fig. S1a), but they differ in the amount of P_2O_5 , which reaches higher values for similar Mg# in the vaugnerites than in the appinites (Fig. S1b). This reflects a higher amount of apatite in the former than in the latter. Granitoids from both associations show lower TiO_2 and P_2O_5 than related mafic rocks, and their trends deflect from those of appinites and vaugnerites. Titanium and P were compatible elements in granitoids, whereas they behaved as incompatible during the evolution of the associated mafic rocks.

6.2 Trace elements

Compatible elements, such as Ni and Cr, reach high values and decrease drastically from ultramafic to mafic appinites (Fig. 7a–b), as a result of the different olivine (Fig. 2a) and chromite modes of the ultramafic cumulates. Vaugnerites follow the same trend, but in most of them Ni and Cr have higher concentrations for similar Mg# than in mafic appinites. Concentrations of Ni and Cr in granitoids from the two associations overlap and plot scattered, particularly those related to appinites (Fig. 7a–b). Incompatible elements (e.g. Rb, Ba, Sr, Nb) have low concentrations in the ultramafic appinites and increase towards mafic appinites and vaugnerites. Both types of mafic rocks display scattered (Fig. 7c–f), but vaugnerites reach higher values of incompatible elements for similar Mg# than most mafic appinites. Most incompatible elements in granitoids show similar contents to those in related mafic rocks. These elements display scattered and overlap between granitoids of both associations, except for Rb, which shows a higher concentration in those associated with vaugnerites (Fig. 7c). Rubidium increases from vaugnerites to related granitoids, whereas it is nearly constant in the granitoids associated with appinites (Fig. 7c). The Rb/Sr ratio vs. Mg# diagram (Fig. S2) illustrates that mafic appinites and vaugnerites show similar Rb/Sr values, and this ratio increases slightly or remains nearly constant with decreasing Mg# in vaugnerites and appinites, respectively (trend 1 and 1' in SI Fig. S2). By contrast, Rb/Sr ratio increases with decreasing Mg# in the granitoids related to vaugnerites and their microgranular enclaves (trend 2 in Fig. S2), while it stays broadly constant in the granitoids associated with appinites.

Total rare-earth elements ($\sum REE$) in Vivero ultramafic appinites range from 17 to 60 times chondrite, with $(La/Yb)_N$ (2.0–7.3), $(La/Nd)_N$ (1.0–1.8) and $(Gd/Yb)_N$ (1.4–2.7). Eu anomaly varies from negative to positive ($Eu/Eu^* = 0.4–1.5$) (Fig. 8a). Mafic appinites are REE enriched (44–70 times chondrite) with respect to ultramafic rocks, especially in heavy REE (HREE) (Fig. 8b). $(La/Yb)_N$ (4.8–5.2), $(La/Nd)_N$ (1.4–1.6) and $(Gd/Yb)_N$ (1.5–1.9) ratios are comparable to those of ultramafics. The Eu anomaly is always negative ($Eu/Eu^* = 0.6–0.8$). Granitoids display a $\sum REE$ range (34–80 times chondrite), which is similar to that of mafic appinites, especially in tonalites and granodiorites (Fig. 8c). Nevertheless, these granitoids differ in having slightly lower HREE, higher REE fractionation: $(La/Yb)_N = 5.2–42$, $(La/Nd)_N = 2.0–2.5$, $(Gd/Yb)_N = 0.9–5.5$ and no Eu anomaly $Eu/Eu^* = 1.1–1.7$). Monzonitic granites stand out as they have lower HREE and significant fractionation between them, with $(Ga/Yb)_N = 4.5–5.5$.

$\sum REE$ are higher in the Bayo–Vigo vaugnerites (55–252 times chondrite) than in appinites. REE patterns are also more fractionated compared to those of appinites (Fig. 8d): $(La/Yb)_N = 10–47$; $(La/Nd)_N = 1.7–2.5$; $(Gd/Yb)_N = 1.7–$

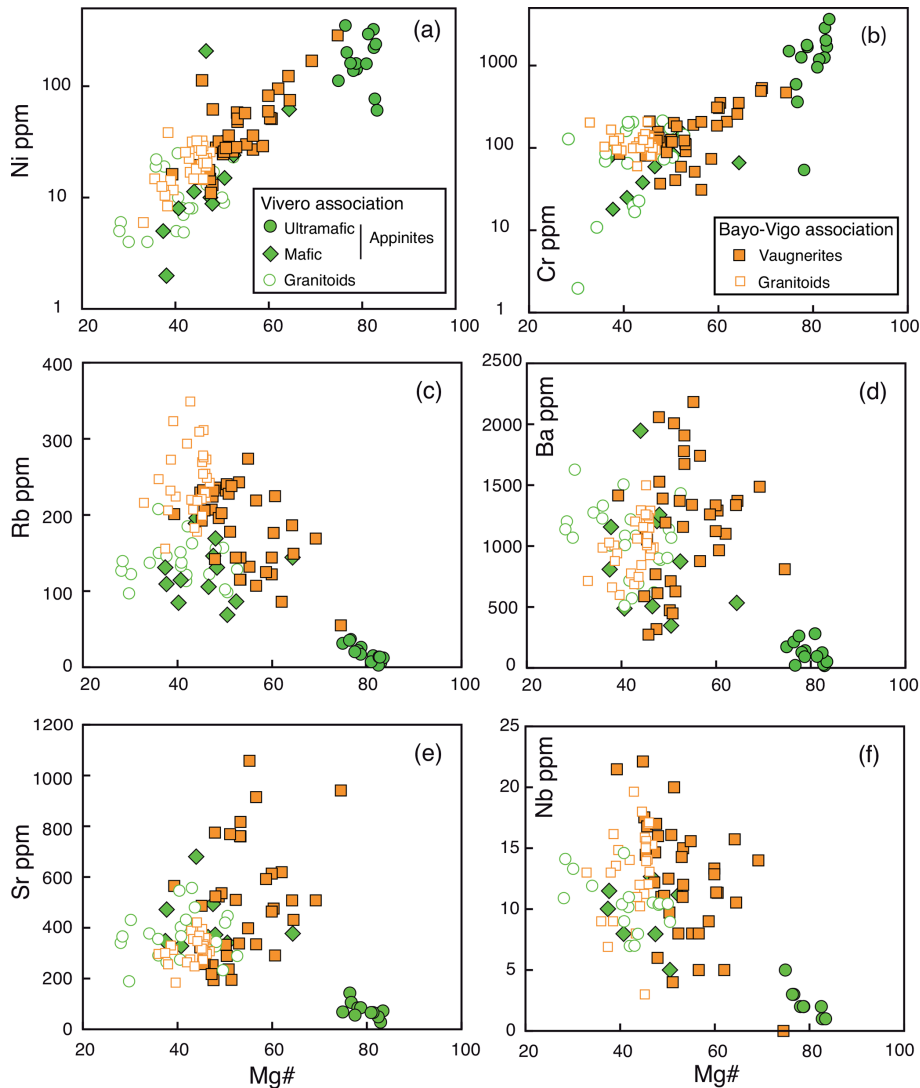


Figure 7. (a–f) Covariation diagrams between different trace elements against Mg# as differentiation index.

5.2). This is due to both light REE (LREE) increase and HREE decrease in the vaugnerites. Eu anomaly is mostly negative ($\text{Eu}/\text{Eu}^* = 0.5\text{--}1.1$). Granodiorites share common REE patterns and are more LREE enriched ($\sum\text{REE} = 103\text{--}179$ times chondrite) and REE fractionated than vaugnerites, with $(\text{La}/\text{Yb})_{\text{N}} = 18\text{--}60$, $(\text{La}/\text{Nd})_{\text{N}} = 2.0\text{--}3.0$ and $(\text{Gd}/\text{Yb})_{\text{N}} = 2.5\text{--}5.0$. The Eu anomaly is invariably negative ($\text{Eu}/\text{Eu}^* = 0.5\text{--}0.9$). Compared with tonalites and granodiorites related to appinites, granodiorites associated with vaugnerites are LREE enriched, whereas their HREE overlap. Only the monzonitic granites related to appinites have similar HREE fractionation to the granodiorites associated with vaugnerites (Fig. 8f). Finally, the monzonitic granites related to vaugnerites show lower $\sum\text{REE}$ (46–110 times chondrite), especially LREE, than the granodiorites and comparable REE fractionation: $(\text{La}/\text{Yb})_{\text{N}} = 18\text{--}46$, $(\text{La}/\text{Nd})_{\text{N}} = 2.3\text{--}2.9$, $(\text{Gd}/\text{Yb})_{\text{N}} = 2.5\text{--}5.0$. Their Eu anomaly

is insignificant or negative ($\text{Eu}/\text{Eu}^* = 0.6\text{--}1.0$). REE patterns of these monzonitic granites compare well with those related to appinites (Fig. 8f).

Multielement diagrams of all these rocks show LILEs, Th and U enrichments and negative Nb and Ti anomalies (Fig. 9a–f). The main differences between the two associations are that the vaugnerite–granitoid one is more enriched in Rb, Th and U and have negative anomalies in Ba, Sr and P (Fig. 9b–f). Differences between rocks of the same association are the following: (i) mafic appinites are LILEs and HFSEs enriched with respect to the ultramafics (Fig. 9b); (ii) the patterns found in granitoids are similar to those in related mafic appinites (Fig. 9c), but the former show the highest LILE and the lowest Ti content; (iii) LILEs increase from tonalites to monzonitic granites, whereas Ti does the opposite; (iv) vaugnerites and related granodiorites show similar multielement diagrams, but the granodiorites have less

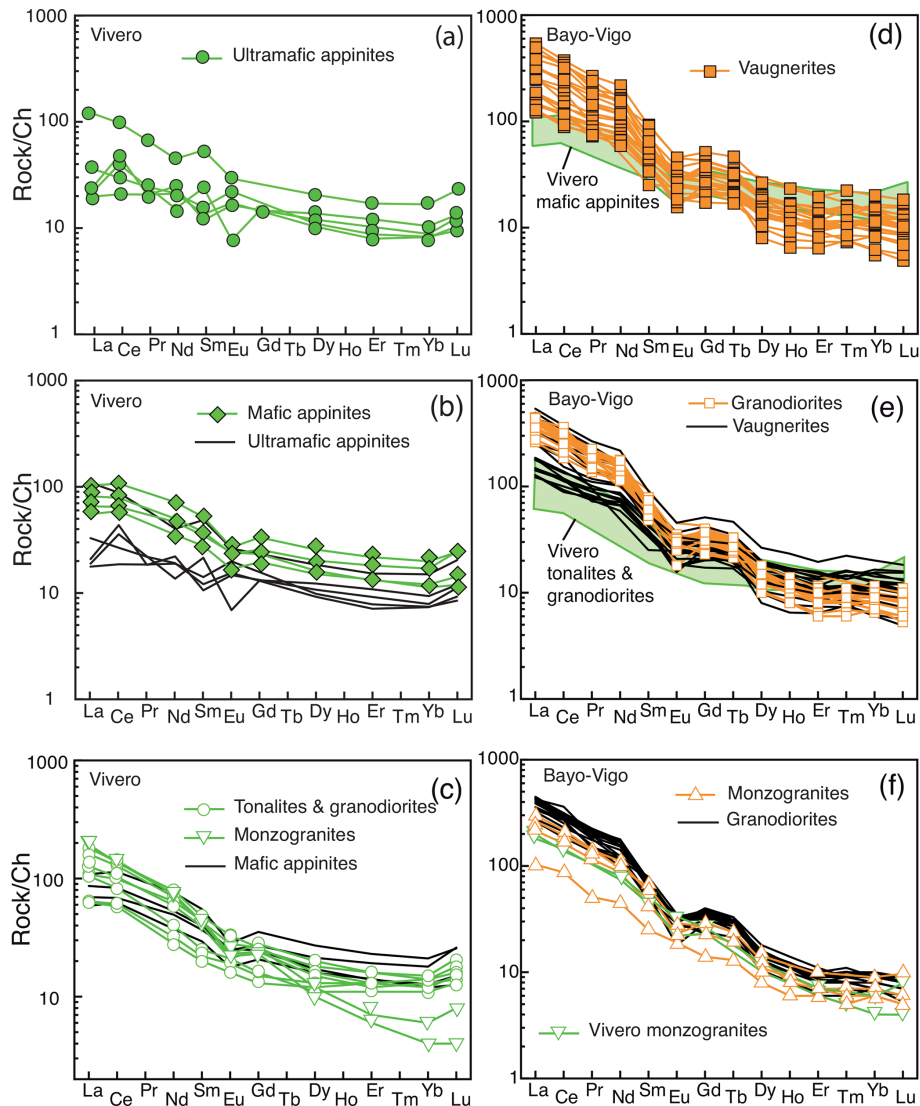


Figure 8. (a) REE patterns of Vivero ultramafic appinites. (b) REE patterns of Vivero mafic appinites with REE patterns of ultramafic appinites in plain solid lines. (c) REE patterns of Vivero granitoids and of mafic appinites (in solid lines) as a reference. (d) REE patterns of Bayo–Vigo vaugnerites. The range for mafic appinites is included as a reference. (e) REE patterns of Bayo–Vigo granodiorites. Patterns of vaugnerites in solid lines; range of Vivero tonalites–granodiorites are also illustrated as a reference. (f) REE patterns of Bayo–Vigo monzonitic granites along with those of granodiorites (in solid lines) and of Vivero monzonitic granites as a reference. Chondritic (Ch) normalisation values of McDonough and Sun (1995).

Ti (Fig. 9d–e); and (v) Ti also decreases in the Bayo–Vigo monzonitic granites with respect to granodiorites (Fig. 9f).

7 Isotopic compositions

Sr and Nd isotopes for the appinite–granitoid association (Galán et al., 1996) were recalculated at 314 Ma (Table S1 in the Supplement), assumed to be the most likely age for the intrusion of granitoids (López-Sánchez et al., 2015) and appinites (see previous comments in the geological setting section). Sr–Nd isotopic results for the vaugnerite–granitoid

association include previously published data (Gallastegui, 2005) (Table S1) and new data (Table 2). All isotopic results for vaugnerites and associated granitoids of Bayo–Vigo were recalculated at the concordant zircon age of 320 Ma (Rodríguez et al., 2007), similar to that of the Vivero association and hence convenient for comparative purposes.

Appinites and related granitoids display very heterogeneous and decoupled Sr–Nd isotopic compositions (Galán et al., 1996). Two ultramafic and one mafic appinites (VGI-2, 5, 13 in Table S1) have variable $\varepsilon_{\text{Sr}_i}$ (27–60) for similar $\varepsilon_{\text{Nd}_i}$ (from –0.1 to –0.3), which led Galán et al. (1996) to suggest a role of H₂O–fluid interaction (Fig. 10a) (Dickin,

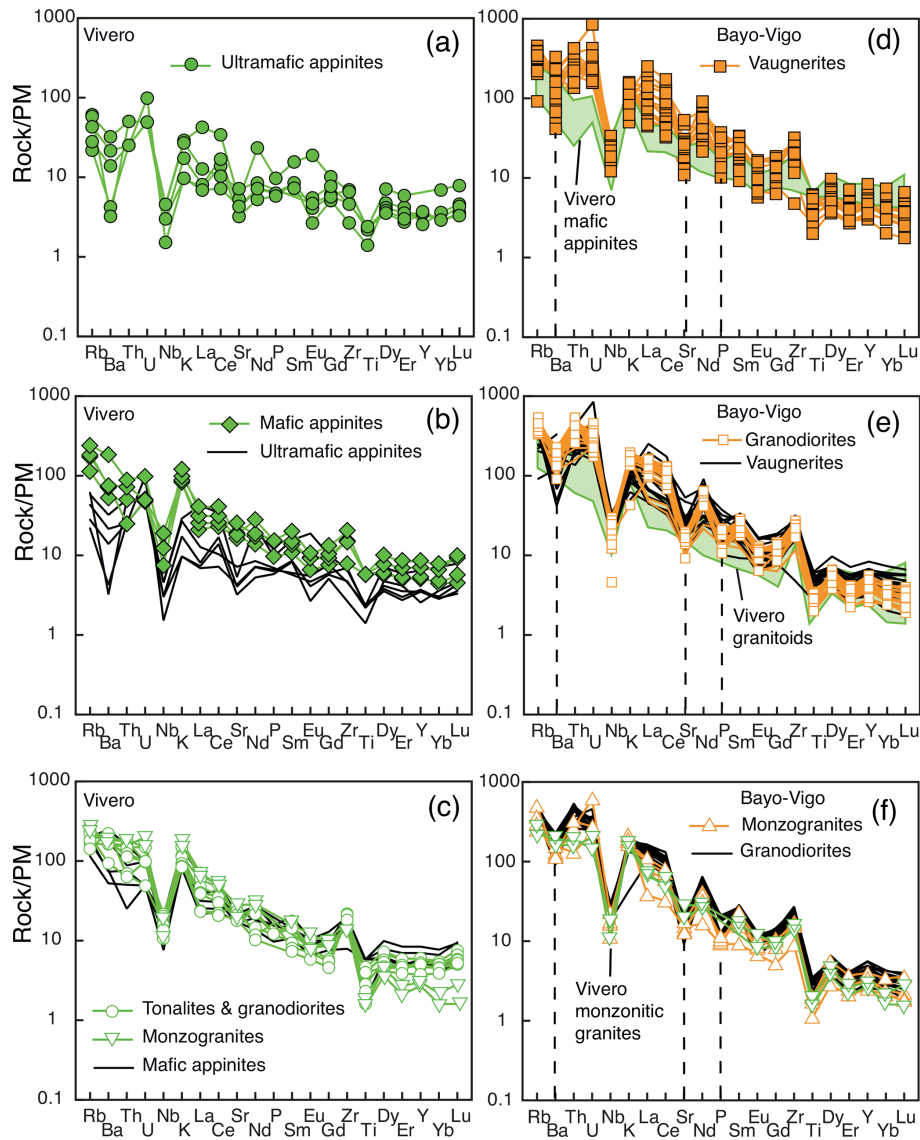


Figure 9. (a) Multi-element diagrams of ultramafic appinites. (b) Multi-element diagrams of mafic appinites with patterns of ultramafic rocks (in solid lines) as a reference. (c) Multi-element diagrams of Vivero granitoids with those of mafic appinites in solid lines as a reference. (d) Multi-element diagrams of vaugnerites with the range of Vivero mafic appinites as a reference. (e) Multi-element diagrams of Bayo–Vigo granodiorites with patterns of vaugnerites (in solid lines) and the range of Vivero tonalites–granodiorites as a reference. (f) Multi-element diagrams of Bayo–Vigo monzonitic granites with patterns of granodiorites (in solid lines) and of Vivero monzonitic granites as a reference. Primitive mantle (PM) normalisation values of McDonough and Sun (1995).

2005, and references therein), not related to post-magmatic perturbations but reflecting complex petrogenesis. Additionally, appinites and related granitoids show considerable compositional overlapping, although the former have higher ϵNd_i and lower ϵSr_i than the latter (ϵNd_i and ϵSr_i for appinites: from -0.1 to -3.9 and 27 – 60 , respectively; ϵNd_i and ϵSr_i for granitoids: from -2.1 to -6.2 and 34 – 61 , respectively) (Fig. 10a–c, Table S1). Moreover, each rock type is heterogeneous. There are five ultramafic appinites (VGI-2, 3, 4, 5, 9) showing Nd isotopes (ϵNd_i : from -0.2 to -1.4) and four of them also Sr isotopes (ϵSr_i : from 29 to 35) within a narrow

range. Two other ultramafics (VGI-6, 11) stand out as having less radiogenic Nd (ϵNd_i : from -2.0 to -2.1) and similar radiogenic Sr (ϵSr_i : 32 – 36). Mafic appinites are even more heterogeneous (Fig. 10a–c). Finally, the most primitive isotopic granitoids are amphibole biotite tonalites with similar ϵNd_i and ϵSr_i to ultramafic and mafic appinites (Fig. 10a; samples VGI-18, 22 in Table S1), whereas the monzonitic granites are the most isotopically evolved, with biotite tonalites and granodiorites having intermediate compositions between the two granitic extremes (Fig. 10a, assimilation with fractional crystallisation, AFC, line).

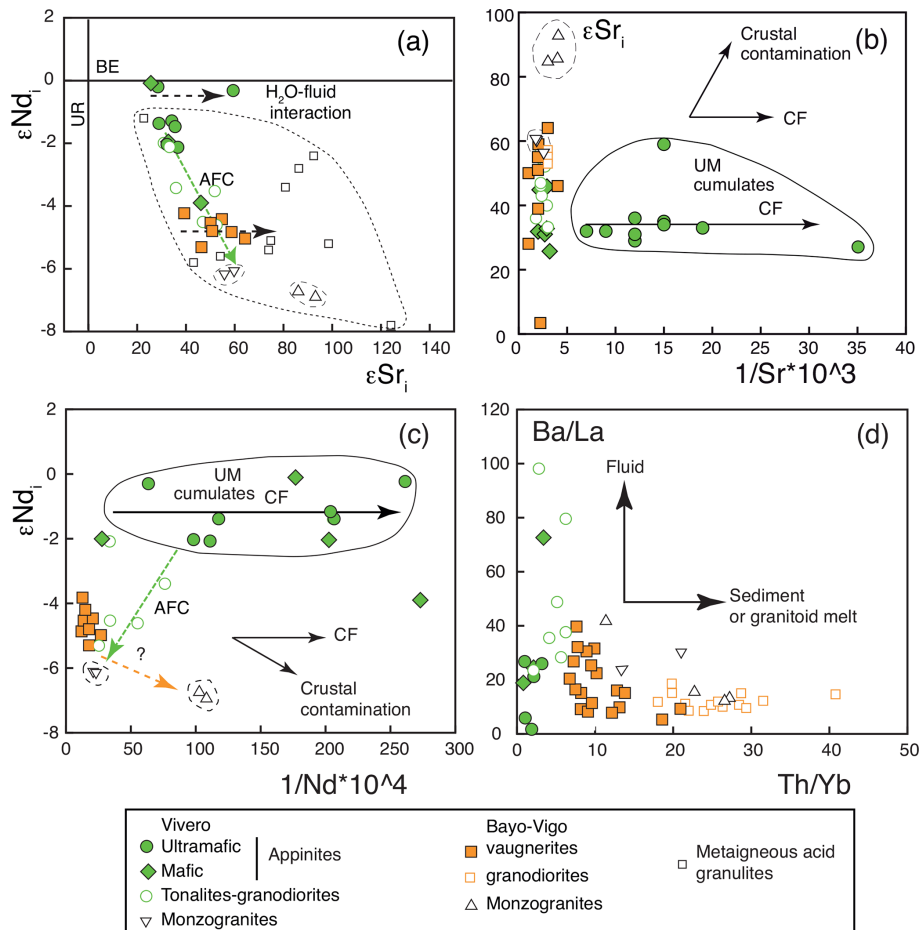


Figure 10. (a) ϵNd_i vs. ϵSr_i diagram. Variable ϵSr for similar ϵNd suggests interaction with H_2O fluids in ultramafic appinites and vaugnerites. The evolutionary trend of granitoids related to appinites is explained by an assimilation with fractional crystallisation (AFC) process. Universal reservoir values after DePaolo (1998). Chondritic universal reservoir values after Hamilton et al. (1983). Monzonitic granites of both examples are encircled with dashed lines. Compositions of metaigneous acid granulites, the likely source of monzonitic granites, after Villaseca et al. (1999); see text. (b) ϵSr_i vs. $1/\text{Sr}$ diagram. (c) ϵNd_i vs. $1/\text{Nd}$ diagram. Trends for crystal fractionation (CF) and crustal contamination are from Jia et al. (2019). Vivero ultramafic appinites follow a clear crystal fractionation (CF) trend. The trend of vaugnerites is not clear. (d) Ba/La vs. Th/Yb diagram showing the trends for fluid and sediment contamination (Woodhead et al., 2001). Appinites follow a fluid contamination trend, whereas vaugnerites seem to follow both contamination by fluids and in some cases by sediments or coeval granitic melts.

Vaugnerites show less radiogenic Nd than most appinites and are more homogeneous between them (ϵNd_i : from -3.8 to -5.3 ; Fig. 10a–c). Other similarities and differences are the following: (i) the $^{87}\text{Sr}/^{86}\text{Sr}_i$ ratios of vaugnerites overlap with those of the appinites, but Sr is more radiogenic in the former (ϵSr_i : 1–71) than in the latter (ϵSr_i : 27–60); (ii) Sr isotopes of vaugnerites are also decoupled with respect to Nd isotopes (reflecting possible interaction with H_2O -rich fluids) (Fig. 10a); (iii) there are no Nd isotopes for the granodiorites related to vaugnerites, but the monzonitic granites differ from those associated with appinites showing higher ϵSr_i and lower ϵNd_i (Fig. 10a–c); and (iv) the vaugneritic trend does not point to related monzonitic granites (Fig. 10a, c).

8 Discussion

8.1 Comparison between the two associations

Similarities between the two case studies are the following: (i) common lithologies among the mafic-intermediate rocks and the granitoid sequence (Fig. 2b–c); (ii) amphibole and/or biotite are the main mafic minerals in both appinites and vaugnerites; (iii) both are magnesian–potassic associations (Fig. 6b); (iv) both have negative anomalies at Nb and Ti with respect to neighbouring elements in multielement diagrams (Fig. 9); and (v) there are crustal isotopic signatures in both appinites and vaugnerites (Fig. 10a). Differences between the two case studies are the following: (i) ultramafic cumulates with olivine and pyroxenes are common in the ap-

pinites and absent in the vaugnerites; (ii) amphibole is either subordinate to biotite or absent in vaugnerites, in contrast to the appinites; (iii) the vaugnerite–granitoid association rocks are more magnesian and enriched in K_2O than those from the appinite–granitoid association (Fig. 6b–d); (iv) the evolution of $K\#$ vs. $Mg\#$ shows positive correlation in vaugnerites and no correlation in appinites; this correlation is reversed in granitoids related to vaugnerites (Fig. 6e); (v) vaugnerites are enriched in P_2O_5 (Fig. S1b), in compatible (Ni, Cr) and incompatible elements (LILEs, Th, U, Nb, LREE), have lower HREE and negative anomalies at Ba, Sr and P, compared to appinites (Figs. 7–9); related granitoids show similar differences in minor and trace elements; (vi) the Rb/Sr ratio is similar in both appinites and vaugnerites, but it stays constant with decreasing $Mg\#$ in the former and tends to increase in the latter (Fig. S2); (vii) the Rb/Sr ratio is higher in granitoids related to vaugnerites than in those associated with appinites (Fig. S2); (viii) Sr isotopic compositions of vaugnerites and appinites overlap, but the former show the least and the most radiogenic Sr; vaugnerites also differ by showing the least radiogenic Nd (Fig. 10a–c); and finally (ix) monzonitic granites of both associations show similar REE patterns, but they differ because those related to vaugnerites have lower ϵNd_i and higher ϵSr_i (Fig. 10a–c).

8.2 Mantle sources

Chemical compositions of mafic minerals in appinites and vaugnerites could be influenced by co-existing melt compositions and solid phases and by crystallisation conditions (viz., T , P , P_{H_2O} , fO_2). Most authors agree that these mafic rocks were derived from mantle basic melts that intruded coevally with related granitoids (Sabatier, 1991; Galán et al., 1996; Gallastegui, 2005; Scarrow et al., 2009a; Couzinié et al., 2014; Pe-Piper and Piper, 2018; Gutiérrez-Alonso et al., 2018). The mantle origin is reflected in concentrations of $SiO_2 < 52$ wt %, $MgO + FeO_T > 12$ wt % and compatible transition elements ($Cr > 250$ ppm, $Ni > 120$ ppm) in the mafic rocks (Figs. 6, 7a–b). The fact that pyroxenes of appinites and vaugnerites differ in their $Mg\#$, along with the presence of olivine only in the appinite suite, suggests that the parental mantle melts were different and might have evolved under different crystallisation conditions. In addition, this is consistent with the different initial Sr–Nd isotopic compositions of the two types of ultramafic–mafic rocks (Fig. 10a, c).

Since ultramafic appinites are cumulates, the composition of the co-existing melts must be inferred from the compositions of cumulus minerals. Olivine was the first phase to crystallise in ultramafic appinites. Its maximum Fo content (or $Mg\# = 82\%$) and the Fe–Mg exchange coefficient between this mineral and the co-existing melt ($K_D = 0.30 \pm 0.03$) (Roeder and Emslie, 1970) were used to estimate the $Mg\#$ of the latter (58 ± 2) (Putirka, 2008). This is within the range of basalt values and similar to the highest $Mg\#$ of

Table 2. Rb, Sr, Sm, and Nd concentrations and isotopic compositions of new samples from Bayo–Vigo vaugnerite–granitoid association. Universal Transverse Mercator (UTM) coordinates are indicated. TCR estimates after Goldstein et al. (1984).

Sample	UTM X	UTM Y	Rb (ppm)	Sr (ppm)	$^{87}Rb/^{86}Sr$	$^{87}Sr/^{86}Sr$	$\pm 2\sigma$	$(^{87}Sr/^{86}Sr)_{20}$	ϵSr_{20}	Sm (ppm)	Nd (ppm)	$^{147}Sm/^{144}Nd$	$^{143}Nd/^{144}Nd$	$\pm 2\sigma$	$(^{143}Nd/^{144}Nd)_{20}$	ϵNd_{20}	TCR (Ga)
Vaugnerites																	
GS-236	520 958.40	4 682 942.08	227	281	2.340	0.7180	0.0080	0.7024	43	7.82	46.82	0.1010	0.512164	0.002000	0.511952	−5.3	1.27
GS-244	520 906.27	4 683 004.37	178	500	1.033	0.7116	0.0050	0.7069	36	8.11	54.47	0.0990	0.512198	0.001800	0.512009	−4.2	1.13
GS-288	499 962.07	4 746 925.81	112	772	0.420	0.7095	0.0070	0.7076	47	9.54	57.17	0.1010	0.512205	0.001800	0.511993	−4.5	1.22
68-18-1	502 821.44	4 777 463.46	153	519	0.853	0.7122	0.0000	0.7083	57	9.48	63.90	0.0897	0.512167	0.000009	0.511980	−4.8	1.16
93-18-2	500 070.95	4 746 930.03	125	488	0.741	0.7111	0.0000	0.7077	49	8.11	51.23	0.0957	0.512182	0.000008	0.511981	−4.8	1.20
223-18-3	520 220.05	4 679 045.22	167	339	1.426	0.7151	0.0000	0.7086	61	6.47	34.20	0.1144	0.512209	0.000007	0.511969	−5.0	1.37
223-18-6	520 205.86	4 679 042.15	152	417	1.055	0.7128	0.0000	0.7080	53	7.42	40.96	0.1095	0.512228	0.000008	0.511999	−4.4	1.28
Granitoids																	
Monzonitic granites																	
223-18-4	520 220.05	4 679 045.22	126	264	1.382	0.7170	0.0000	0.7107	91	1.90	8.90	0.1294	0.512146	0.000008	0.511874	−6.9	1.71
223-18-5	520 220.05	4 679 045.22	158	261	1.753	0.7182	0.0000	0.7102	84	2.19	9.46	0.1398	0.512173	0.000008	0.511880	−6.7	1.88

Vivero mafic appinites (Fig. 6e). Clinopyroxene compositions in appinites and vaugnerites do not discriminate the alkaline or subalkaline affinity of their parental basaltic melts (Fig. 5a). Regarding the whole-rock alkali abundances, the appinite basaltic melts are expected to be subalkaline to transitional (Fig. 6a). Interestingly, in ultramafic appinites, clinopyroxene has higher Mg# (84–94) than olivine (68–82), despite both minerals being among the earliest phases to crystallise as they are included by orthopyroxene and especially by Amp 1 and phlogopite (Fig. 3a, c). Several hypotheses could be envisaged to account for this difference: (i) the Mg–Fe cation exchange reaction between olivine and clinopyroxene, whose partition coefficient [$K_{D_{Fe/Mg}}^{Ol/Cpx} = (Fe/Mg)_{Ol}/(Fe/Mg)_{Cpx}$] is strongly dependent on temperature (Loucks, 1996); (ii) subsolidus re-equilibration between the two minerals (Antonicelli et al., 2020); (iii) reactive melt flow through a melt-poor olivine-rich crystal mush (Antonicelli et al., 2020) or, alternatively, mixing between an earlier olivine bearing magma and a new melt injection (Galán et al., 2017), both processes causing olivine dissolution; and (iv) increasing P_{H_2O} during the crystallisation of the ultramafic appinites. Firstly, increasing $K_{D_{Fe/Mg}}^{Ol/Cpx}$ with decreasing temperature during the crystallisation of a basaltic system could explain higher Mg# in clinopyroxene than in olivine. However, this dependence is limited to systems with water content < 3 wt % (see below), which include plagioclase co-existing with olivine, clinopyroxene, orthopyroxene and melt (Loucks, 1996); plagioclase is almost absent in ultramafic appinites, where amphibole dominates. Secondly, subsolidus re-equilibration between olivine and clinopyroxene is not likely: both phases are usually as isolated inclusions mainly within Amp-1 type crystals, which have similar Mg# (64–86) to that of olivine. The re-equilibration is more probable between olivine and Amp 3 forming pseudomorphs after olivine and especially after clinopyroxene. However, Amp 3 has a Mg# range (78–93) more similar to that of clinopyroxene than to that of olivine. In addition, there is no evidence of recrystallisation in ultramafic appinites (e.g. granoblastic microstructures or subsolidus equilibrium temperatures; Antonicelli et al., 2020). The two-pyroxene thermometer provides equilibrium temperatures of 938 ± 35 °C for Vivero ultramafic appinites (Galán, 1987), which are over the solidus of a H₂O-saturated basaltic system at 0.5 GPa (e.g. Green 1982), the estimated pressure for the emplacement of these rocks (Galán, 1987). Thirdly, reactive melt flow through a melt-poor olivine-rich crystal mush causing olivine dissolution and the formation of the other mafic phases (Antonicelli et al., 2020) may have occurred, but there is no evidence of it (e.g. host olivine-rich rocks or melt–peridotite reaction at the contact zone). Alternatively, mixing between different mantle melts in a magma chamber was suggested for the origin of other Iberian ultramafic appinites (Galán et al., 2017), but no evidence of this process (e.g. spinel zoning) exists in the Vivero ultramafic appinites. In such a scenario, dissolution

of olivine crystals from an earlier magma might appear when they get in contact with a new more primitive melt giving clinopyroxene with higher Mg#. It is worth noting that if any of these two reactive processes took place, subsequent magmatic evolution should have occurred at increasing H₂O concentration to explain the high amphibole mode. This is documented experimentally for subalkaline basalts with high water content (Gaetani et al., 1993): pyroxenes are followed by amphibole in the crystallisation sequence, not by plagioclase. Finally, increasing H₂O concentration over 3 wt % during the clinopyroxene crystallisation with respect to that of olivine could explain higher Mg# of the former (hypothesis iv): higher water content might trigger increasing fO_2 , leading to simultaneous magnetite and clinopyroxene formation (Table 1). Earlier crystallisation of olivine from an initial hydrous, but perhaps subsaturated melt, and/or H₂O assimilation during the magma ascent could explain this P_{H_2O} increasing and, therefore, saturation of the magmatic system. Hypothesis (iv) is supported by hydrous experimental data on phase relations and compositions in a basaltic system (Gaetani et al., 1993; Feig et al., 2006). High volatile content is characteristic of most appinite suites worldwide (Murphy, 2013). The origin of this water could be predominantly juvenile (i.e. an inherited character of the mantle melt itself) (Castro et al., 2003, 2010), but later H₂O increasing by contamination from the host rock during the magma ascent is also possible (Galán et al., 1996; Roberts et al., 2000; Murphy, 2013; Bea et al., 2021). Interestingly, partial melting of a hydrated mantle could have contributed not only to generate hydrous basaltic melts, but also to focus strain and cause nucleation of lithospheric-scale strike-slip shear zones (Vaughan and Scarrow, 2003), such as the ones related to the NW Iberian appinites and vaugnerites (Vivero and Malpica–Lamego shear zones, respectively). These shear zones might have facilitated the ascent of these mafic magmas (Atherton and Ghani, 2002) and potentially have promoted further interaction of them with crustal H₂O fluids. In addition, assimilation of crustal H₂O fluids by the appinite magmatic system might contribute to its saturation and significantly shift its solidus temperature to lower values. This fact could explain the following: (i) the embayed and skeletal crystals of olivine; they would not be the result of dissolution, but of supercooling (MacKenzie et al., 1982; Vernon, 2004); (ii) the general transformation of clinopyroxene and olivine into amphibole forming pseudomorphs (Amp-3 crystals; Fig. 3a); and (iii) decoupling of ϵS_i and ϵNd_i due to increasing ϵSr_i at constant ϵNd_i in one of the Vivero ultramafic appinites (Fig. 10a). Thus, the trend followed by the Vivero appinites in the Ba/La vs. Th/Yb diagram (Fig. 10d) could corroborate both an origin from partial melting of a hydrous metasomatised mantle and differentiation processes, mainly dominated by crystal fractionation, taking place under high P_{H_2O} . This trend is characterised by increasing Ba/La ratio at constant Th/Yb values, the variation in the latter ratio being more influenced by sediment input (Woodhead et al., 2001). In sum-

mary, either hypotheses (iii) or (iv) could explain compositional and microstructural characteristics of ultramafic appinites, but whatever the case, differentiation of these rocks must have taken place under high $P_{\text{H}_2\text{O}}$.

Olivine was not found in the Bayo–Vigo vaugnerites, although it could have been completely pseudomorphosed by amphibole \pm biotite \pm Cr-rich spinel clots (Sabatier, 1991; Gallastegui, 2005). Compared to appinites, vaugnerites have higher Mg# and K_2O contents (Fig. 6b, d–e), and the most mafic terms have a transitional–alkaline geochemistry (Fig. 6a). Hence, they might derive from mantle melts more akin to calc–alkaline lamprophyres of spessartite or kersantite types (Sabatier, 1991). Early biotite fractionation from such parental melts would explain the positive correlation between K# and Mg# values (Fig. 6e) and possibly the negative anomaly at Ba in these rocks (Fig. 9d). Interestingly, pyroxenes in vaugnerites show lower Mg# values than in ultramafic appinites. This observation, along with the fact that plagioclase appears earlier in the crystallisation sequence of vaugnerites (as inclusions in earlier amphibole and biotite; Fig. 4a–b), points to lower $P_{\text{H}_2\text{O}}$ during the crystallisation of vaugnerites than that of the ultramafic appinites. Moreover, earlier crystal fractionation of plagioclase could also have contributed to the characteristic negative anomalies at Ba and Sr of vaugnerites (Fig. 9d–e). Nevertheless, interaction with H_2O fluids during the metasomatism of the vaugnerite mantle protolith previous to its melting and/or during the vaugnerite magma ascent is reflected in the U enrichment with respect to Th (U is considered more mobile than Th in aqueous fluids; Fig. 9d) (Schmidt et al., 2004; Kessel et al., 2005), in the increasing Ba/La ratio at constant Th/Yb ratio displayed by most of vaugnerites (Fig. 10d), and possibly in their variable εSr_i for similar εNd_i (Fig. 10a). Interestingly, a few vaugnerites display the opposite trend in Fig. 10d: increasing Th/Yb ratio at constant Ba/La ratio. This suggests either input of sediments and/or sediment-derived melts during the mantle metasomatism (Woodhead et al., 2001), or later mingling and mixing with crustal melts comparable to the associated granitoids. The latter hypothesis is more probable as this trend is defined by vaugnerites cropping out as microgranular enclaves in monzonitic granites or as interlayered bands with granodiorites showing intense mingling and mixing at the contacts.

Several hypotheses exist to explain the heterogeneous crustal isotopic signature of appinites and vaugnerites. All of them agree that a mix of mantle and crustal components must have occurred, but they differ over the depth and time at which mixing took place. These hypotheses are the following: (i) the parental melt was isotopically depleted, or close to bulk-earth composition, and later contaminated by crustal components (namely H_2O fluids and/or partial melts) during the ascent (Galán et al., 1996); (ii) the mantle source was previously metasomatised in a supra-subduction zone (Roberts et al., 2000; Castro et al., 2003; Bonin, 2004; Scarrow et al., 2009a; Zhang et al., 2012; von Raumer et al., 2014;

Couziñé et al., 2016). The subduction-type mantle metasomatism could be early Variscan (von Raumer et al., 2014; Couziñé et al., 2016) or older (Janoušek et al., 2000; Vilà et al., 2005; Scarrow et al., 2009a). In an alternative interpretation, the basic melts derived from such metasomatised mantle interacted with felsic crustal material during their ascent through the crust (Sabatier, 1991; Fowler et al., 2008; Scarrow et al., 2009b; Kuvínová et al., 2017; Bea et al., 2021) or even at the intrusion level; (iii) melting of a tectonically imbricated mixture of mantle and crustal rocks took place either in an earlier Variscan subduction zone or at the lower crust–mantle interface (Bea et al., 1999, 2021; Castro et al., 2003, 2010; López-Moro and López-Plaza, 2004); and finally (iv) that melting of a subduction-related metasomatised mantle took place with minor involvement of asthenospheric melts (Jia et al., 2019).

Crustal contamination of depleted mantle melts during their ascent (hypothesis i) is more likely for the appinites (Galán et al., 1996) than for the vaugnerites, because the latter have much lower εNd_i than depleted mantle melts (Fig. 10a). Nevertheless, the mantle melts of appinites could not have been highly depleted, otherwise the necessary contamination by crustal components would also have increased their SiO_2 contents to higher values than those observed. Therefore, a source with the isotopic composition similar to the bulk earth would be more likely for Vivero appinites than a mid-ocean ridge basalt (MORB)-type depleted mantle. However, shifting of their εSr_i to the right of the bulk earth suggests that this type of source interacted with H_2O -rich fluids (Galán et al., 1996). Also, the presence of quartz \pm feldspar ocelli (Fig. 4f) could support the hypothesis of interaction with crustal magmas during their ascent. They could be xenocrysts or xenoliths derived from this acid crustal component. However, these ocelli are rare in the appinites, suggesting that crustal melts (Fig. 10d) did not affect their differentiation trend much. Consequently, most appinites follow nearly horizontal trends in the εSr_i vs. $1/\text{Sr}$ and εNd_i vs. $1/\text{Nd}$ diagrams (Fig. 10b–c), reflecting crystal fractionation from basic melts with similar εSr_i and very close εNd_i values. Crystal fractionation is also supported by the evidence of increasing REE from ultramafic to mafic appinites (Fig. 8a–b). By contrast, vaugnerites follow neither a crystal fractionation trend nor a clear mixing trend (Fig. 10a–c). Their low εNd_i , along with high number of both compatible and incompatible elements (Fig. 7a–b, d–f), supports the hypothesis that they originated from partial melting of a subduction-type metasomatised mantle. However, common quartz \pm feldspar ocelli in vaugnerites (Fig. 4f) could have resulted from further interaction between vaugneritic magmas and crustal material during the ascent and emplacement (hypotheses ii–iii).

At present, we consider hypothesis (ii) or hypothesis (iii) (mentioned above) as the most realistic interpretations to account for the geochemical and isotope data of both appinites and vaugnerites, i.e. melting of subduction-type metasoma-

tised mantle, with further interaction of the resulting basic melts with crustal materials (Fig. 10a–d) at the lower crust and/or during their ascent and emplacement. Nevertheless, based on higher values of Mg#, K#, P₂O₅, (La/Yb)_N, (Gd/Yb)_N and higher contents of compatible elements in the vaugnerites compared to the appinites (Figs. 6e, 7, 8, 9 and S1b in the Supplement), it is suggested that their metasomatised mantle sources were different: a fertile peridotite source (e.g. amphibole-bearing spinel lherzolites) for appinites and a more refractory peridotite source, with amphibole, phlogopite ± apatite ± garnet, for vaugnerites. The role of phlogopite in the mantle source of vaugnerites is experimentally demonstrated by Condamine et al. (2022). Their results could explain the characteristic negative anomaly at Ba with respect to Rb of vaugnerites (Fig. 9d), implying mantle partial melting at $P < 3$ GPa. In addition, stronger REE and HREE fractionation in the vaugnerites might be related to higher partition coefficients for HREE–middle(M)REE than for LREE of residual garnet in the mantle source. Also, vaugneritic melts co-existing with garnet would have inherited lower Sm/Nd ratios than appinitic melts derived from amphibole spinel peridotites. Thus, time-integrated ¹⁴³Nd/¹⁴⁴Nd ratios would be lower in vaugnerites than in appinites (Fig. 10a). Similar differences in the mantle source and depth of melting have also been suggested for Variscan vaugnerites and less potassic calc–alkaline gabbro–diorites, comparable to appinites, in Corsica (Cocherie et al., 1994; Ferré and Leake, 2001).

Vaugnerite primary melts might have interacted with crustal components during their ascent and emplacement. In addition to quartz–feldspar ocelli (Fig. 4f), further textural evidence of this interaction is provided by the following: (i) partially resorbed or skeletal calcic plagioclase cores and plagioclase crystals with complex zoning, displaying sharp gaps in An composition (Figs. 3f, 4d–e); and (ii) amphibole ± biotite clots including clinopyroxene relics (Fig. 4c) (Castro, 2001; Baxter and Feely, 2002; Janoušek et al., 2004; Molina et al., 2012; Pietranik and Koepke, 2014; Ubide et al., 2014). The felsic crustal component could have been coeval granitic magmas, which would explain their geochemical affinity with vaugneritic mafic rocks. Thus, granitoids related to vaugnerites show more alkalis (Fig. 6a), magnesian–potassic character (Fig. 6b), higher Rb/Sr ratio (Fig. S2), and REE, Th and U abundances (Figs. 8–9) than those related to appinites. In addition, REE and multielement patterns of most granitoids and associated appinites or vaugnerites are alike (Figs. 8–9). Finally, the Rb/Sr vs. Mg# trend of vaugneritic microgranular enclaves is similar to that of the host granitoids (Fig. S2), suggesting that the evolution of vaugneritic magmas was deeply influenced by the interaction with coeval granitic melts (Gallastegui, 2005). Interaction of appinite and vaugnerite magmas with the metamorphic country rocks at the level of emplacement were not observed as the contacts are usually sharp and intrusive.

The data of this study indicate lithospheric mantle sources, at different depths, greatly refertilised by crustal components in a supra-subduction setting, as the origin of the studied mafic magmatism. The involvement of asthenospheric melts in the generation of NW Iberian appinites and vaugnerites (hypothesis iv by Jia et al., 2019) does not seem likely. Notwithstanding this, after slab break-off, asthenospheric upsurge onto metasomatised lithospheric mantle (von Raumer et al., 2014; Laurent et al., 2017) could have triggered partial melting in both lithospheric mantle and lower crust imbrications, either in an accretionary prism or in the lower crust. This could produce syn- to post-collisional mafic–granitic magmatism, as has been proposed for other collisional orogens elsewhere (viz., Alps, Caledonides) (Davies and von Blanckenbourg, 1995; Atherton and Ghani, 2002).

In summary, we prefer the hypothesis of melting of a subduction-type metasomatised mantle as the origin of the two types of high Mg–K mafic rocks studied: appinites and vaugnerites. This mantle was most likely heterogeneous, and melting must have occurred at different depths. The Bayo–Vigo vaugnerites could form by partial melting of a deeper, more refractory and enriched in phlogopite subcontinental lithospheric mantle than the Vivero appinites, the source of which could be a rather more fertile peridotite (e.g. amphibole-bearing spinel lherzolites). The resulting hydrous basic melts could further interact with crustal H₂O-rich fluids and possibly the associated granitoids, during their ascent and emplacement. Therefore, it is inferred that the post-collisional metasomatised lithospheric mantle was heterogeneous across the Variscan NW Iberian Massif. This could be the case in other post-collisional settings where different types of high K–Mg mafic magmatism have been observed.

8.3 Crustal sources

The granitoid sequence of Vivero shows a typical AFC trend in the ϵNd_i vs. ϵSr_i diagram (Fig. 10a). This process would have operated at deep levels. Some tonalites show isotopic compositions comparable to those of appinites, whereas others have a more evolved isotopic signature but similar major element compositions. This led Galán et al. (1996) to suggest the involvement of different mafic end-members in the AFC process. This process would have started with appinitic melts, followed by another hybrid but more evolved mafic magmas which, after interaction with the crustal component, would have given rise to isotopically more evolved tonalites and granodiorites. The hybrid character of tonalites is also reflected in the compositions of relic clinopyroxene in amphibole clots, similar to those of ultramafic appinites. Monzonitic granites are considered representative of the crustal end component in this AFC process, because they show the most evolved isotopic composition and strong fractionation of HREE ((Gd/Yb)_N = 4.5–5.5; Fig. 8c), which suggests equilibrium with a garnet-rich residue. The HREE fractionation would have been erased if the monzogranitic

melts had interacted with more mafic ones (Galán et al., 1996). The equilibrium of the monzonitic granites with a garnet-rich residue is consistent with their high Sr/Y (33–43) and $(\text{La}/\text{Yb})_{\text{N}}$ (32–41) ratios. If this hypothesis is assumed, the crustal-end component in the AFC process was characterised by moderately low $\varepsilon\text{Nd}_{314}$ (–6) and relatively low radiogenic Sr ($^{87}\text{Sr}/^{86}\text{Sr}_{314} = 0.708$). Therefore, only crustal rocks with moderate time-integrated Rb/Sr and with moderate LREE enrichment, such as greywackes and/or acid-intermediate metaigneous rocks, could be the crustal source. A pure crustal origin is also assumed for the monzonitic granites related to vaugnerites: they show comparable REE patterns to those of Vivero and more evolved Sr–Nd isotopic compositions (Fig. 10a–c). Their high Sr/Y (13–28), $(\text{La}/\text{Yb})_{\text{N}}$ (18–45) and $(\text{Gd}/\text{Yb})_{\text{N}}$ (2.5–5.0) ratios are also consistent with a garnet bearing source. The Bayo–Vigo granodiorites show similar radiogenic Sr to vaugnerites but are less radiogenic than the monzonitic granites (Fig. 10b). Although Nd isotopic compositions are not available for these granodiorites, their high Sr/Y (9.0–27), $(\text{La}/\text{Yb})_{\text{N}}$ (34–60) and $(\text{Gd}/\text{Yb})_{\text{N}}$ (2.3–5.0) ratios and peraluminous character are also consistent with partial melting of a crustal garnet bearing source. However, the possibility that their origin was related to mixing at depth between vaugnerite-forming and monzonitic granite-forming magmas cannot be completely ruled out.

Available Sr–Nd isotopic data for possible crustal sources of the monzonitic granites indicate that only some metaigneous acid granulites would fulfil the requirements for both cases. These granulites (Fig. 10a) could be similar to xenoliths found in post-Variscan lamprophyres of the Central Iberian Zone (Fig. 10a), which are isotopically very heterogeneous (Villaseca et al., 1999). The crustal residence ages of these xenoliths ($T_{\text{CR}} = 1.52 \pm 0.27$ Ma, 1 s) (Goldstein et al., 1984) overlap those of Vivero (1.37 ± 0.02 Ma) and Bayo–Vigo (1.79 ± 0.12 Ma) monzogranites. However, differences between the monzonitic granites of the two associations considered here (viz., more aluminous biotites for similar Mg, higher K#, Mg#, Rb, Rb/Sr, Th/Yb and $^{87}\text{Sr}/^{86}\text{Sr}_i$ ratios, and lower εNd_i in those related to vaugnerites than in those associated with appinites) indicate either greater involvement of metasediments or of biotite incongruent melting in the origin of the former.

9 Conclusions

The following conclusions have been drawn from comparing the two most representative Variscan post-collisional Mg–K mafic rocks (appinites and vaugnerites) and their respective associated granitoids in the NW Iberian Massif.

Similarities are as follows: (i) common mafic-intermediate and granitoid lithologies, (ii) dominant amphibole and/or biotite as mafic minerals, (iii) negative anomalies at Nb–Ti typical of calc–alkaline rocks, and (iv) crustal Sr–Nd isotopic

signature of mafic-intermediate rocks. The main differences are as follows: (i) amphibole-rich cumulates are frequent in appinites and rare in vaugnerites; (ii) the appinite–granitoid association is calc–alkalic, whereas the vaugnerite–granitoid one is calc–alkalic transitional to alkali–calcic and has higher Mg and K numbers than the appinitic–granitoid association; (iii) vaugnerites are more enriched in compatible and incompatible trace elements than appinites; (iv) LREE / HREE ratios and fractionation between HREE are also more marked in vaugnerites than in appinites; (v) related granitoids display similar differences in trace elements except from the most evolved monzonitic granites, which show comparable REE patterns in both associations; and (vi) vaugnerites differ from appinites in having lower εNd_i and more variable εSr_i .

Appinites and vaugnerites are the result of interaction processes between mantle and crust materials at two main levels: firstly, in a supra-subduction zone, where the mantle experienced metasomatism prior to partial melting, and subsequently at the lower crust and during the ascent and emplacement of the resulting melts. The two types of Mg–K mafic rocks were formed by different mantle melts, the former by subalkaline to transitional basalts and the latter by basic melts akin to calc–alkaline lamprophyres. The mantle source of these parental melts was heterogeneous. Neodymium isotopic compositions of appinites would be close to the bulk earth, but Sr isotopic composition would be more radiogenic, possibly by interaction with H₂O-rich fluids. The vaugneritic mantle source would have less radiogenic Nd than that of appinites. Trace elements, especially REE patterns and fractionation between them, in appinites and vaugnerites, also point to different mineral modes of the mantle source and different depths of partial melting. Amphibole spinel lherzolites are the inferred sources for appinites, whereas more refractory peridotites with amphibole and phlogopite ± garnet ± apatite are the inferred sources for vaugnerites. These differences imply that the subcontinental lithospheric mantle resulting from the Variscan collision differs from external terrains, such as the West Asturian–Leonese Zone, where the studied appinites are located, towards more internal Galicia–Trás-os-Montes Zone, where the vaugnerites crop out.

Isotopic evidence of crystal fractionation as a differentiation process is shown by the ultramafic appinites. This process took place near the level of emplacement at the middle crust. However, fractionation of biotite, along with plagioclase, from the vaugnerite melts would also explain their typical positive correlation between Mg# and K#. Moreover, variation in εSr_i at nearly constant εNd_i of both appinites and vaugnerites could indicate H₂O–fluid interaction. This interaction might take place during the subduction-type metasomatism of the mantle protolith. Hence, it is highly likely that the pristine mafic melts formed by partial melting of this protolith were hydrous, but assimilation of H₂O-rich fluids might have also occurred during their ascent through the

crust, along lithospheric-scale strike-slip shear zones and by interaction with coeval granitoids.

Granitoids related to appinites follow an AFC trend, with the mafic end similar to appinites and the crustal component comparable to the most evolved monzonitic granites. The most likely crustal source of the monzonitic granite melts was metaigneous acid granulites. The same source is deduced for the monzonitic granites related to vaugnerites, without discarding the involvement either of metasediments in this source or an increasing role of biotite incongruent melting. Melting of these granulites could have been enhanced by the intrusion of the Mg–K mafic magmas at the lower crust. Compositional characteristics of granodiorites associated with vaugnerites are also consistent with a pure crustal origin, but the possibility of hybridisation with vaugnerite melts at depth cannot be ruled out.

Data availability. Mineral and whole-rock analyses are compiled from references mentioned in the article (see the Introduction section) and available on request from the authors. Previously published isotopic data and recalculated ages and parameters are in the Supplement. New isotopic data are reported in the article.

Supplement. The supplement related to this article is available online at: <https://doi.org/10.5194/ejm-35-845-2023-supplement>.

Author contributions. All authors contributed to the study conception and design. Sample material was prepared and data was collected and analysed by Gumer Galán, Gloria Gallastegui, Andrés Cuesta and Luis González-Menéndez. The first draft of the manuscript was written by Gumer Galán, and all authors commented on subsequent versions of the manuscript. The final version was read and approved by all authors.

Competing interests. The contact author has declared that none of the authors has any competing interests.

Disclaimer. Publisher's note: Copernicus Publications remains neutral with regard to jurisdictional claims made in the text, published maps, institutional affiliations, or any other geographical representation in this paper. While Copernicus Publications makes every effort to include appropriate place names, the final responsibility lies with the authors.

Acknowledgements. The authors thank Claire Reed for the correction of English spelling and grammar and for improving the style on an earlier version of the manuscript. They are also indebted to the *European Journal of Mineralogy* associated editor, Riccardo Tribuzio, for taking care of the manuscript and for his helpful comments and to Carlos Villaseca, Jean-François Moyen and Maria Rosaria Renna, whose suggestions and remarks were

very useful in improving earlier versions of the manuscript. Finally, they are grateful for the technical and human support provided by SGIker of UPV/EHU and European funding (ERDF and ESF) for the isotopic analyses.

Financial support. This research was carried out within the framework of the following research projects: Government of Asturias and FEDER funds GEO-TEC (FC-GRUPIN-IDI/2018/000216 and AYUD/2021/51293) and Spanish Ministerio de Ciencia e Innovación (CGL2011-26700 and PID2019-109018RB-100).

Review statement. This paper was edited by Riccardo Tribuzio and reviewed by Jean-François Moyen, Carlos Villaseca, and Maria Rosaria Renna.

References

- Antonicevli, M., Tribuzio, R., Liu, T., and Wu, F.-Y.: Contaminating melt flow in magmatic peridotites from the lower continental crust (Rocca d'Argimonia sequence, Ivrea–Verbano Zone), *Eur. J. Mineral.*, 32, 587–612, <https://doi.org/10.5194/ejm-32-587-2020>, 2020.
- Atherton, M. P. and Ghani, A. A.: Slab breakoff: a model for Caledonian, Late Granite syn-collisional magmatism in the orthotectonic (metamorphic) zone of Scotland and Donegal, *Lithos*, 62, 65–85, [https://doi.org/10.1016/S0024-4937\(02\)00111-1](https://doi.org/10.1016/S0024-4937(02)00111-1), 2002.
- Bailey, E. B. and Maufe, H. B.: The Geology of Ben Nevis and Glen Coe and the Surrounding Country (Explanation of Sheet 53), *Memoirs of the Geological Survey, Scotland*, 53, 167 pp., 1916.
- Baxter, S. and Feely, M.: Magma mixing and mingling in granitoids: examples from the Galway Granite, Connemara, Ireland, *Miner. Petrol.*, 76, 63–74, <https://doi.org/10.1007/s007100200032>, 2002.
- Bea, F., Montero, P., and Molina, J. F.: Mafic Precursors, Peraluminous Granitoids, and Late Lamprophyres in the Avila Batholith: a Model for the Generation of Variscan Batholith in Iberia, *J. Geol.*, 107, 399–419, <https://doi.org/10.1086/314356>, 1999.
- Bea, F., Gallastegui, G., Montero, P., Molina, F. J., Scarrow, J., Cuesta, A., and González-Menéndez, L.: Contrasting high-Mg, high-K rocks in Central Iberia: the appinite–vaugnerite conundrum and their (non-existent) relation with arc magmatism, *J. Iber. Geol.*, 47, 235–261, <https://doi.org/10.1007/s41513-020-00152-x>, 2021.
- Bonin, B.: Do coeval mafic and felsic magmas in post-collisional to within-plate regimes necessarily imply two contrasting, mantle and crustal, sources? A review, *Lithos*, 78, 1–24, <https://doi.org/10.1016/j.lithos.2004.04.042>, 2004.
- Cambeses, A., Molina, J. F., Morales, I., Lázaro, C., Moreno, J. A., Montero, P., and Bea, F.: Compositional Evolution of the Variscan Intra-Orogenic Extensional Magmatism in the Valencia del Ventoso Plutonic Complex, Ossa-Morena Zone (SW Iberia): A View from Amphibole Compositional Relationships, *Minerals-Basel*, 11, 431, <https://doi.org/10.3390/min11040431>, 2021.

- Capdevila, R.: Le métamorphisme régional progressif et les granites dans le segment hercynien de Galice Nord Orientale (NW de l'Espagne), PhD Thèse, Univ. Montpellier, 430 pp., 1969.
- Castro, A.: Plagioclase morphologies in assimilation experiments. Implications for disequilibrium melting in the generation of granodiorite rocks, *Miner. Petrol.*, 71, 31–49, <https://doi.org/10.1007/s007100170044>, 2001.
- Castro, A., Corretgé, L. G., De La Rosa, J. D., Fernández, C., López, S., García-Moreno, O., and Chacón, H.: The Appinite-Migmatite Complex of Sanabria; NW Iberian Massif, Spain, *J. Petrol.*, 44, 1309–1344, <https://doi.org/10.1093/petrology/44.7.1309>, 2003.
- Castro, A., Gerya, T., García-Casco, A., Fernández, C., Díaz-Alvarado, J., Moreno-Ventas, I., and Löw, I.: Melting Relations of MORB–Sediment Mélanges in Underplated Mantle Wedge Plumes; Implications for the Origin of Cordilleran-type Batholiths, *J. Petrol.*, 51, 1267–1295, <https://doi.org/10.1093/petrology/egq019>, 2010.
- Cocherie, A., Rossi, P., Fouillac, A. M., and Vidal, P.: Crust and mantle contributions to granite genesis – An example from the Variscan batholith of Corsica, France, studied by trace-element and Nd–Sr–O-isotope systematics, *Chem. Geol.*, 115, 173–211, [https://doi.org/10.1016/0009-2541\(94\)90186-4](https://doi.org/10.1016/0009-2541(94)90186-4), 1994.
- Condamine, P., Couzinié, S., Fabbrizio, A., Devidal J.-L., and Médard, E.: Trace element partitioning during incipient melting of phlogopite-peridotite in the spinel and garnet stability fields, *Geochim. Cosmochim. Ac.*, 327, 53–78, <https://doi.org/10.1016/j.gca.2022.04.011>, 2022.
- Corretgé, L. G., Suárez, O., Galán, G., and Fernández-Suárez, J.: Zona Asturoccidental Leonesa. Magmatismo, in: *Geología de España*, edited by: Vera, J. A., Sociedad Geológica de España, Instituto Geológico y Minero, Madrid, 63–68, ISBN 84-7840-546-1, 2004.
- Couzinié, S., Moyen, J.-F., Villaros, A., Paquette, J.-L., Scarrow, J. H., and Marignac, C.: Temporal relationships between Mg–K mafic magmatism and catastrophic melting of the Variscan crust in the southern part of Velay Complex (Massif Central, France), *J. Geosci.-Czech.*, 59, 69–86, <https://doi.org/10.3190/jgeosci.155>, 2014.
- Couzinié, S., Laurent, O., Moyen, J.-F., Zeh, A., Bouilhol, P., and Villaros, A.: Post-collisional magmatism: Crustal growth not identified by zircon Hf–O isotopes, *Earth Planet. Sc. Lett.*, 456, 182–195, <https://doi.org/10.1016/j.epsl.2016.09.033>, 2016.
- Cuesta, A. and Gallastegui, G.: Zona Centro Ibérica. Magmatismo: Galicia Occidental, in: *Geología de España*, edited by: Vera, J. A., Sociedad Geológica de España, Instituto Geológico y Minero, Madrid, 96–100, ISBN 84-7840-546-1, 2004.
- Dallmeyer, R. D., Martínez Catalán, J. R., Arenas, R., Gil Ibarguchi, J. I., Gutiérrez Alonso, G., Farias, P., Bastida, F., and Aller, J.: Diachronous Variscan tectonothermal activity in the NW Iberian Massif: Evidence from $^{40}\text{Ar}/^{39}\text{Ar}$ dating of regional fabrics, *Tectonophysics*, 277, 307–337, [https://doi.org/10.1016/S0040-1951\(97\)00035-8](https://doi.org/10.1016/S0040-1951(97)00035-8), 1997.
- Davies, J. H. and von Blanckenbourg, F.: Slab breakoff: A model of lithosphere detachment and its test in the magmatism and deformation of collisional orogens, *Earth Planet. Sc. Lett.*, 129, 85–102, [https://doi.org/10.1016/0012-821X\(94\)00237-S](https://doi.org/10.1016/0012-821X(94)00237-S), 1995.
- DePaolo, D. J.: Neodymium Isotope Geochemistry: An Introduction, in: *Minerals and Rocks 20*, edited by: Wyllie, P. J., Elsevier, Amsterdam, 187 pp., ISBN 3-642-48918-4, 1998.
- Dickin, A. P.: *Radiogenic Isotope Geology*. Cambridge University Press, Cambridge, 471 pp., ISBN 0-521-8231-1, 2005.
- Díez-Balda, M. A., Vegas, R., and González Lodeiro, F.: Structure of the Autochthon of the Central Iberian Zone, in: *Pre-Mesozoic Geology of Iberia*, edited by: Dallmeyer, R. D. and Martínez, E., Springer-Verlag, Heidelberg, 172–188, <https://doi.org/10.1007/978-3-642-83980-1>, 1990.
- Díez Fernández, R., Martínez Catalán, J. R., Arenas Martín, R., and Abati Gómez, J.: Tectonic evolution of a continental subduction-exhumation channel: Variscan structure of the basal allochthonous units in NW Spain, *Tectonics*, 30, 1–22, <https://doi.org/10.1029/2010TC002850>, 2011.
- Díez Fernández, R., Arenas Martín, R., Pereira, M. F., Sánchez-Martínez, S., Albert, R., Martín Parra, L.-M., Rubio Pascual, F.-J., and Matas, J.: Tectonic evolution of Variscan Iberia: Gondwana–Laurussia collision revisited, *Earth-Sci. Rev.*, 162, 269–292, <https://doi.org/10.1016/j.earscirev.2016.08.002>, 2016.
- Errandonea-Martín, J., Sarrionandia, F., Carracedo-Sánchez, M., Gil Ibarguchi, J. I., and Eguífluz, L.: Petrography and geochemistry of late- to post-Variscan vaugnerite series rocks and calc-alkaline lamprophyres within a cordierite-bearing monzogranite (Sierra Bermeja Pluton, southern Iberian Massif), *Geol. Acta*, 16, 237–255, <https://doi.org/10.1344/GeologicaActa2018.16.3.1>, 2018.
- Farias, P., Gallastegui, G., González Lodeiro, F., Marquínez, J., Martín Parra, L. M., Martínez Catalán, J. R., Pablo Maciá, J. G., and Rodríguez Fernández, L. R.: Aportaciones al conocimiento de la litoestratigrafía y estructura de Galicia Central, *Memórias No. 1*, Museu e Laboratório Mineralógico e Geológico, Faculdade de Ciências, Universidade do Porto, 1, 411–431, 1987.
- Feig, S. T., Koepke, J., and Snow, J. E.: Effect of water on tholeiitic basalt phase equilibria: an experimental study under oxidizing conditions, *Contrib. Mineral. Petr.*, 152, 611–638, <https://doi.org/10.1007/s00410-006-0123-2>, 2006.
- Fernández-Suárez, J., Dunning, G. R., Jenner, G. A., and Gutiérrez-Alonso, G.: Variscan collisional magmatism and deformation in NW Iberia: constraints from U–Pb geochronology of granitoids, *J. Geol. Soc. Lond.*, 157, 565–576, <https://doi.org/10.1144/jgs.157.3.565>, 2000.
- Ferré, E. C. and Leake, B. E.: Geodynamic significance of early orogenic high-K crustal and mantle melts: example of the Corsica Batholith, *Lithos*, 59, 47–67, [https://doi.org/10.1016/S0024-4937\(01\)00060-3](https://doi.org/10.1016/S0024-4937(01)00060-3), 2001.
- Fowler, M. and Rollinson, H.: Phanerozoic sanukitoids from Caledonian Scotland: Implications for Archean subduction, *Geology*, 40, 1079–1082, <https://doi.org/10.1130/G33371.1>, 2012.
- Fowler, M. B., Kocks, H., Darbyshire, D. P. F., and Greenwood, P. B.: Petrogenesis of high Ba–Sr plutons from the Northern Highlands Terrane of the British Caledonian Province, *Lithos*, 105, 129–148, <https://doi.org/10.1144/jgs.157.3.565>, 2008.
- Frost, B. R., Barnes, C. G., Collins, W. J., Arculus, R. J., Ellis, D. J., and Frost, D. C.: A Geochemical Classification for Granitic Rocks, *J. Petrol.*, 42, 2033–2048, <https://doi.org/10.1093/petrology/42.11.2033>, 2001.
- Gaetani, G. A., Grove, T. L., and Bryan, W. B.: The influence of water on the petrogenesis of subduction-related igneous rocks, *Nature*, 365, 332–334, <https://doi.org/10.1038/365332a0>, 1993.

- Galán, G.: Las rocas graníticas del Macizo de Vivero en el sector norte (Lugo, NO de España). *Corpus Geologicum Gallaeciae*, Segunda Serie III, Academia de Ciencias Gallega, Laboratorio Geológico de Lage, Fundación Pedro Barrie de la Maza, La Coruña, 376 pp., ISBN 84-85728-64-5, 1987.
- Galán, G., Pin, C., and Duthou J.-L.: Sr–Nd isotopic record of multi-stage interactions between mantle-derived magmas and crustal components in a collision context – The ultramafic–granitoid association from Vivero (Hercynian belt, NW Spain), *Chem. Geol.*, 131, 67–91, [https://doi.org/10.1016/0009-2541\(96\)00027-7](https://doi.org/10.1016/0009-2541(96)00027-7), 1996.
- Galán, G., Oliveras, V., and Paterson, B.: Thermal and redox state of the subcontinental lithospheric mantle of NE Spain from thermobarometric data on mantle xenoliths, *Int. J. Earth Sci.*, 100, 81–106, <https://doi.org/10.1007/s00531-009-0503-8>, 2011.
- Galán, G., Enrique, P., Butjosa, L., and Fernández-Roig, M.: Spinels of Variscan olivine hornblendites related to the Montnegre granitoids revisited (NE Spain): petrogenetic evidence of mafic magma mixing, *Geol. Acta*, 15, 323–336, <https://doi.org/10.1344/GeologicaActa2017.15.4.5>, 2017.
- Gallastegui, G.: *Petrología del macizo granodiorítico de Bayo-Vigo (provincia de Pontevedra, España)*. Serie Nova Terra, 26. Edicions do Castro, Sada, A Coruña, 412 pp., ISBN 8485-175-3, 2005.
- Gallastegui, G., Corretgé, L. G., and Cuesta, A.: *Petrografía y aspectos geoquímicos de los enclaves microgranudos de Cangas de Morrazo-Moaña (Prov. de Pontevedra)*, *Cad. Lab. Xeol. Laxe*, 7, 55–85, Ediciós Do Castro, Sada, A Coruña, ISBN 84-7492-204-6, 1984.
- Gil Ibarguchi, J. I.: A comparative study of vaugnerites and metabasic rocks from the Finisterre region (NW Spain), *Neues Jb. Miner. Abh.*, 143, 91–101, 1981.
- Gil Ibarguchi, J. I., Bowden, P., and Whitley, J. E.: Rare Earth Element Distribution in Some Hercynian Granitoids from the Finisterre Region, NW Spain, *J. Geol.*, 92, 397–416, <https://doi.org/10.1086/628875>, 1984.
- Goldstein, S. L., O’Nions, R. K., and Hamilton, P. J.: A Sm–Nd isotopic study of atmospheric dust and particulates from major river systems, *Earth Planet. Sc. Lett.*, 70, 221–236, [https://doi.org/10.1016/0012-821X\(84\)90007-4](https://doi.org/10.1016/0012-821X(84)90007-4), 1984.
- González-Menéndez, L., Gallastegui, G., Cuesta, A., Montero, P., Valverde-Vaquero, P., Rubio-Ordóñez, A., and Bea, F.: Los primeros pulsos del magmatismo Varisco del NO de Iberia (Galicia, España). Datos preliminares de nuevas edades U–Pb SHRIMP y CA–ID–TIMS en granodioritas precoces, in: *Geotemas*, 18, p. 430, X Congreso Geológico de España, 5–7 Julio 2021, 2021.
- Green T. H.: Anatexis of mafic crust and high pressure crystallisation of andesites, in: *Andesites: Orogenic andesites and related rocks*, edited by: Thorpe R. S., Chichester, John Wiley and Sons, New York, 465–488, ISBN 0-471-28034-8, 1982.
- Guo, Z., Wilson, M., Zhang, L., Zhang, M., Cheng, Z., and Liu, J.: The role of subduction channel mélanges and convergent subduction systems in the petrogenesis of post-collisional K-rich mafic magmatism in NW Tibet, *Lithos*, 198–199, 184–201, <https://doi.org/10.1016/j.lithos.2014.03.020>, 2014.
- Gutiérrez-Alonso, G., Collins, A. S., Fernández-Suárez, J., Pastor-Galán, D., González-Clavijo, E., Jourdan, F., Weil, A. B., and Johnston, S. T.: Dating of lithospheric buckling: $^{40}\text{Ar}/^{39}\text{Ar}$ ages of syn-orocline strike-slip shear zones in northwestern Iberia, *Tectonophysics*, 643, 44–54, <https://doi.org/10.1016/j.tecto.2014.12.009>, 2015.
- Gutiérrez-Alonso, G., Fernández-Suárez, J., López-Carmona, A., and Gärtner, A.: Exhuming a cold case: The early granodiorites of the northwest Iberian Variscan belt – A Visean magmatic flare-up?, *Lithosphere-US*, 10, 194–216, <https://doi.org/10.1130/L706.1>, 2018.
- Hamilton, P. J., O’Nions, R. K., Bridgwater, D., and Nutman, A.: Sm–Nd studies of Archaean metasediments and metavolcanics from West Greenland and their implications for the Earth’s early history, *Earth Planet. Sc. Lett.*, 62, 263–272, [https://doi.org/10.1016/0012-821X\(83\)90089-4](https://doi.org/10.1016/0012-821X(83)90089-4), 1983.
- Hawthorne, F. C., Oberti, R., Harlow, G. E., Maresch, W. V., Martin, R. F., Schumacher, J. C., and Welch, M. D.: Nomenclature of amphibole supergroup, *Am. Mineral.*, 97, 2031–2048, <https://doi.org/10.2138/am.2012.4276>, 2012.
- Irvine, T. N. and Baragar, W. R. A.: A guide to the chemical classification of the common volcanic rocks, *Can. J. Earth Sci.*, 8, 523–548, <https://doi.org/10.1139/e71-055>, 1971.
- Janoušek, V., Bowes, D. R., Rogers, G., Farrow, C. M., and Jelínek, E.: Modelling Diverse Processes in the Petrogenesis of a Composite Batholith: the Central Bohemian Pluton, Central European Hercynides, *J. Petrol.*, 41, 511–543, <https://doi.org/10.1093/petrology/41.4.511>, 2000.
- Janoušek, V., Braithwaite, C. J. R., Bowes, D. R., and Gerdes, A.: Magma-mixing in the genesis of Hercynian calc-alkaline granitoids: an integrated petrographic and geochemical study of the Sázava intrusion, Central Bohemian Pluton, Czech Republic, *Lithos*, 78, 67–99, <https://doi.org/10.1016/j.lithos.2004.04.046>, 2004.
- Jia, L., Wang, L., Wang, G., Lei, S., and Wu, X.: Petrogenesis of the Late Triassic shoshonitic Shadegai pluton from the northern North China Craton: Implications for crust-mantle interaction and post-collisional extension, *Geosci. Front.*, 10, 595–610, <https://doi.org/10.1016/j.gsf.2018.08.002>, 2019.
- Kessel, R., Schmidt, M. W., Ulmer, P., and Pettke, T.: Trace element signature of subduction-zone fluids, melts and supercritical liquids at 120–180 km depth, *Nature*, 437, 724–727, <https://doi.org/10.1038/nature03971>, 2005.
- Key, C. H.: Origin for appinitic pockets in the diorites of Jersey. Channel Islands, *Mineral. Mag.*, 41, 183–192, <https://doi.org/10.1180/minmag.1977.041.318.05>, 1977.
- Klötzli, U. S., Sinigoi, S., Quick, J. E., Demarchi, G., Tassinari, C. C. G., Sato, K., and Günes, Z.: Duration of igneous activity in the Sesia Magmatic System and implications for high-temperature metamorphism in the Ivrea–Verbano deep crust, *Lithos*, 206–207, 19–33, <https://doi.org/10.1016/j.lithos.2014.07.020>, 2014.
- Kuno, H.: Lateral variation of basalt magma types across continental margins and island arcs, *B. Volcanol.*, 29, 195–222, <https://doi.org/10.1007/BF02597153>, 1966.
- Kuvínová, S., Faryad, S. V., Verner, K., Schimiz, M., and Holub, F.: Ultrapotassic dykes in the Moldanubian Zone and their significance for understanding of the post-collisional mantle dynamics during Variscan orogeny in the Bohemian Massif, *Lithos*, 272–273, 205–221, <https://doi.org/10.1016/j.lithos.2016.12.007>, 2017.
- Lameyre, J. and Bowden, P.: Plutonic rock types series: discrimination of various granitoid series and related rocks, *J. Vol-*

- canol. Geoth. Res., 14, 169–186, [https://doi.org/10.1016/0377-0273\(82\)90047-6](https://doi.org/10.1016/0377-0273(82)90047-6), 1982.
- Laurent, O., Couzinié, S., Zeh, A., Vanderhaeghe, O., Moyer, J.-F., Villaros, A., Gardien, V., and Chelle-Michou, C.: Protracted, coeval crust and mantle melting during Variscan late-orogenic evolution: U–Pb dating in the eastern French Massif Central, *Int. J. Earth Sci.*, 106, 421–451, <https://doi.org/10.1007/s00531-016-1434-9>, 2017.
- Le Maitre, R. W. (Ed.): *Igneous Rocks: A Classification and Glossary of Terms Recommendations of the International Union of Geological Sciences, Sub-Commission on the Systematics of Igneous Rocks*, Cambridge University Press, Cambridge, 236 pp., <https://doi.org/10.1017/CBO9780511535581>, 2002.
- Leterrier, J., Maury, R. C., Thonon, P., Girard, D., and Marchal, M.: Clinopyroxene composition as a method of identification of the magmatic affinities of Paleo-volcanic series, *Earth Planet. Sc. Lett.*, 59, 139–154, [https://doi.org/10.1016/0012-821X\(82\)90122-4](https://doi.org/10.1016/0012-821X(82)90122-4), 1982.
- Llana Fúnez, S. and Marcos, A.: The Malpica-Lamego Line: a major crustal-scale shear zone in the Variscan belt of Iberia, *J. Struct. Geol.*, 23, 1015–1030, [https://doi.org/10.1016/S0191-8141\(00\)00173-5](https://doi.org/10.1016/S0191-8141(00)00173-5), 2001.
- López-Moro, F.-J. and López-Plaza, M.: Monzonitic series from the Variscan Tormes Dome (Central Iberian Zone): petrogenetic evolution from monzogabbro to granite magmas, *Lithos*, 72, 19–44, <https://doi.org/10.1016/j.lithos.2003.08.002>, 2004.
- López-Sánchez, M. A., Marcos, A., Martínez, F. J., Iriando, A., and Llana-Fúnez, S.: Setting new constraints on the age of crustal-scale extensional shear zone (Vivero fault): implications for the evolution of Variscan orogeny in the Iberian massif, *Int. J. Earth Sci.*, 104, 927–962, <https://doi.org/10.1007/s00531-014-1119-1>, 2015.
- Loucks, R. R.: A precise olivine-augite Mg-Fe exchange geothermometer, *Contrib. Mineral. Petr.*, 125, 140–150, 1996.
- MacDonald, G. A.: Composition and origin of Hawaiian lavas, in: *Studies in volcanology: A memoir in honour of Howel Williams*, edited by: Coats, R. R., Hay, R. L., and Anderson, C. A., *Geol. Soc. Am. Mem.*, 116, 477–522, <https://doi.org/10.1130/MEM116>, 1968.
- MacKenzie, W. S., Donaldson, C. H., and Guilford, C.: *Atlas of Igneous Rocks and Their Textures*, Longman, London, 142 pp., ISBN 0582300827, 1982.
- Marcos, A.: Un nuevo mapa geológico de la parte septentrional del Domo de Lugo (Galicia oriental, NO de España): implicaciones sobre la estratigrafía, estructura y evolución tectónica del Manto de MondonPedo, *Trabajos Geol.*, Universidad de Oviedo, 33, 171–200, 2013.
- Martínez Catalán, J. R.: Estratigrafía y estructura del domo de Lugo (sector oeste de la zona asturoccidental-leonesa). *Corpus Geologicum Gallaeciae, Segunda Serie II. Fundación Pedro Barrié de la Maza, La Coruña*, 324 pp., ISBN 84-85728-45-9, 1985.
- McDonough, W. F. and Rudnick, R.: Mineralogy and composition of the upper mantle, in: *Ultrahigh Pressure Mineralogy: Physics and Chemistry of the Earth's Deep Interior*, edited by: Hemley, R. J., *Rev. Mineral.*, 37, 139–164, Mineralogical Society of America, Washington DC, <https://doi.org/10.1515/9781501509179-006>, 1998.
- McDonough, W. F. and Sun, S.-S.: The composition of the Earth, *Chem. Geol.*, 120, 223–253, [https://doi.org/10.1016/0009-2541\(94\)00140-4](https://doi.org/10.1016/0009-2541(94)00140-4), 1995.
- Michel-Lévy, A. and Lacroix, A.: Sur le granite à amphibole de Vaugneray (Vaugnérite de Fournet), *B. Soc. Fr. Minéral.*, 10, 27–31, 1887.
- Molina, J. F., Scarrow, J. H., Montero, P. G., and Bea, F.: High-Ti amphibole as a petrogenetic indicator of magma chemistry: evidence for mildly alkalic-hybrid melts during evolution of Variscan basic–ultrabasic magmatism of Central Iberia, *Contrib. Mineral. Petr.*, 158, 69–98, <https://doi.org/10.1007/s00410-008-0371-4>, 2009.
- Molina, J. F., Montero, P., Bea, F., and Scarrow, J. H.: Anomalous xenocryst dispersion during tonalite–granodiorite crystal mush hybridization in the mid crust: Mineralogical and geochemical evidence from Variscan appinites (Avila Batholith, Central Iberia), *Lithos*, 153, 224–242, <https://doi.org/10.1016/j.lithos.2012.03.021>, 2012.
- Montel, J. M. and Weisbrod, A.: Characteristics and evolution of “vaugneritic magmas”: an analytical and experimental approach, on the example of the Cévennes Médiannes (French Massif Central), *B. Minéral.*, 109, 575–587, 1986.
- Murphy, B. J.: Appinite suites: A record of the role of water in the genesis, transport, emplacement and crystallization of magma, *Earth-Sci. Rev.*, 119, 35–59, <https://doi.org/10.1016/j.earscirev.2013.02.002>, 2013.
- Nachit, H., Razafimahefa, N., Stussi, J. M., and Caron, J. P.: Composition chimique des biotites et typologie magmatique des granitoids, *C.R. Acad. Sci. II*, 301, 813–818, 1985.
- Pe-Piper, G. and Piper, D. J. W.: The Jeffers Brook diorite–granodiorite pluton: style of emplacement and role of volatiles at various crustal levels in Avalonian appinites, Canadian Appalachians, *Int. J. Earth Sci.*, 107, 863–883, <https://doi.org/10.1007/s00531-017-1536-z>, 2018.
- Pietranik, A. and Koepke, J.: Plagioclase transfer from a host granodiorite to mafic microgranular enclaves: diverse records of magma mixing, *Miner. Petrol.*, 108, 681–694, <https://doi.org/10.1007/s00710-014-0326-6>, 2014.
- Pin, C. and Bassin, C.: Evaluation of a strontium-specific extraction chromatographic method for isotopic analysis in geological materials, *Anal. Chim. Acta*, 269, 249–255, [https://doi.org/10.1016/0003-2670\(92\)85409-y](https://doi.org/10.1016/0003-2670(92)85409-y), 1992.
- Pin, C. and Santos Zalduegui, J. F.: Sequential separation of light rare-earth elements, thorium and uranium by miniaturized extraction chromatography: Application to isotopic analyses of silicate rocks, *Anal. Chim. Acta*, 339, 79–89, [https://doi.org/10.1016/s0003-2670\(96\)00499-0](https://doi.org/10.1016/s0003-2670(96)00499-0), 1997.
- Putirka, K. D.: Thermometers and Barometers for Volcanic Systems, in: *Mineral, Inclusions and Volcanic Processes*, edited by: Putirka, K. D. and Tepley, F., *Rev. Mineral. Geochem.*, 69, Mineralogical Soc. Am., Washington DC, 61–120, <https://doi.org/10.2138/rmg.2008.69.3>, 2008.
- Reche, J., Martínez, F. J., and Arboleya, M. L.: Low- to medium-pressure Variscan metamorphism in Galicia (NW Spain): evolution of a kyanite-bearing synform and associated bounding antiformal domains, in: *What Drives Metamorphism and Metamorphic Reactions?*, edited by: Treloar, P. J. and O'Brian, P. J., *Special Publication*, 138, *Geol. Soc. London*, 61–79, <https://doi.org/10.1144/GSL.SP.1996.138.01.05>, 1998.

- Rickwood, P. C.: Boundary lines within petrologic diagrams which use oxides of major and minor elements, *Lithos*, 22, 247–263, [https://doi.org/10.1016/0024-4937\(89\)90028-5](https://doi.org/10.1016/0024-4937(89)90028-5), 1989.
- Roberts, M., Pin, C., Clemens, J. D., and Paquette, J.-L.: Petrogenesis of Mafic to Felsic Plutonic Rock Associations: the Calc-alkaline Quérigut Complex, French Pyrenees, *J. Petrol.*, 41, 809–844, <https://doi.org/10.1093/ptrology/41.6.809>, 2000.
- Rodríguez, J., Gil Iburguchi, J., and Paquette, J.: Sincroniãa del magmatismo varisco en el Macizo Ibeirico: nuevas edades U-Pb en granitoides de la regioin de Finisterre (La Coruña, España), in: XV Semana – VI Congreso Ibeirico de Geoquímica, Vila Real, Portugal, 16–21 July 2007, DVD-ROM, 146–149, ISBN 978-972-669-805-0, 2007.
- Roeder, P. L. and Emslie, R. F.: Olivine-Liquid Equilibrium, *Contrib. Mineral. Petr.*, 29, 275–289, <https://doi.org/10.1007/BF00371276>, 1970.
- Sabatier, H.: Vaugnerites et granites magnésiens dans le Massif Central français: une association particulière des roches grenues acides et basiques, Thèse d'État, Univ P. et M. Curie, Paris, 559 pp., 1984.
- Sabatier, H.: Vaugnerites: Special lamprophyre-derived mafic enclaves in some Hercynian granites from Western and Central Europe, in: Enclaves and granite petrology, edited by: Didier, J. and Barbarin, B., *Dev. Petrol.*, 13, Elsevier, Amsterdam, 63–81, ISBN 0444891455, 1991.
- Scarrow, J. H., Bea, F., Montero, P., and Molina, J. F.: Shoshonites, vaugnerites and potassic lamprophyres: similarities and differences between “ultra”-high-K rocks, *Earth Env. Sci. T. R. So.*, 99, 159–175, <https://doi.org/10.1017/S1755691009008032>, 2009a.
- Scarrow, J. H., Molina, J. F., Bea, F., and Montero, P.: Within-plate calc-alkaline rocks: Insights from alkaline mafic magmageraluminous crustal melt hybrid appinites of the Central Iberian Variscan continental collision, *Lithos*, 110, 50–64, <https://doi.org/10.1016/j.lithos.2008.12.007>, 2009b.
- Schmidt, M. W., Vielzeuf, D., and Auzanneau, E.: Melting and dissolution of subducting crust at high pressures: the key role of white mica, *Earth Planet. Sc. Lett.*, 228, 65–84, <https://doi.org/10.1016/j.epsl.2004.09.020>, 2004.
- Steiger, R. H. and Jäger, E.: Subcommittee on geochronology: Convention on the use of decay constants in geo and cosmochronology, *Earth Planet. Sc. Lett.*, 36, 359–362, [https://doi.org/10.1016/0012-821X\(77\)90060-7](https://doi.org/10.1016/0012-821X(77)90060-7), 1977.
- Tanaka, T., Togashi, S., Kamioka, H., Amakawa, H., Kagami, H., Hamamoto, T., Yuhara, M., Orihashi, Y., Yoneda, S., Shimizu, H., Kunimaru, T., Takahashi, K., Yanagi, T., Nakano, T., Fujimaki, H., Shinjo, R., Asahara, Y., Tanimizu, M., and Dragusanu, C.: JNdi-1: a neodymium isotopic reference in consistency with LaJolla neodymium, *Chem. Geol.*, 168, 279–281, [https://doi.org/10.1016/S0009-2541\(00\)00198-4](https://doi.org/10.1016/S0009-2541(00)00198-4), 2000.
- Ubide, T., Galé, C., Arranz, E., Lago, M., and Larrea, P.: Clinopyroxene and amphibole crystal populations in a lamprophyre sill from the Catalanian Coastal Ranges (NE Spain): A record of magma history and a window to mineral-melt partitioning, *Lithos*, 184, 225–242, <https://doi.org/10.1016/j.lithos.2013.10.029>, 2014.
- Vaughan, A. P. and Scarrow, J. H.: K-rich mantle metasomatism control of localization and initiation of lithospheric strike-slip faulting, *Terra Nova*, 15, 163–169, <https://doi.org/10.1046/j.1365-3121.2003.00485.x>, 2003.
- Vernon, R. H.: A Practical Guide to Igneous Microstructure, Cambridge University Press, Cambridge, 594 pp., <https://doi.org/10.1017/CBO9780511807206>, 2004.
- Vilà, M., Pin, C., Enrique, P., and Liesa, M.: Telescoping of three distinct magmatic suites in an orogenic setting: Generation of Hercynian igneous rocks of the Albera Massif (Eastern Pyrenees), *Lithos*, 83, 97–127, <https://doi.org/10.1016/j.lithos.2005.01.002>, 2005.
- Villaseca, C., Downes, H., Pin, C., and Barbero, L.: Nature and Composition of the Lower Continental Crust in Central Spain and the Granulite–Granite Linkage: Inferences from Granulitic Xenoliths, *J. Petrol.*, 40, 1465–1496, <https://doi.org/10.1093/ptrology/40.10.1465>, 1999.
- von Raumer, J. F., Finger, F., Veselá, P., and Stampfli, G. M.: Durbachites–Vaugnerites – a geodynamic marker in the central European Variscan orogen, *Terra Nova*, 26, 85–95, <https://doi.org/10.1111/ter.12071>, 2014.
- Wang, X., Zhang, J., Rushmer, T., Adam, J., Turner, S., and Xu, W.: Adakite-Like Potassic Magmatism and Crust-Mantle Interaction in a Postcollisional Setting: An Experimental Study of Melting Beneath the Tibetan Plateau, *J. Geophys. Res.-Sol. Ea.*, 124, 12782–12798, <https://doi.org/10.1029/2019JB018392>, 2019.
- Wasserburg, G. J., Jacobsen, S. B., DePaolo, D. J., McCulloch, M. T., and Wen, T.: Precise determination of ratios, Sm and Nd isotopic abundances in standard solutions, *Geochim. Cosmochim. Ac.*, 45, 2311–2323, [https://doi.org/10.1016/0016-7037\(81\)90085-5](https://doi.org/10.1016/0016-7037(81)90085-5), 1981.
- Wells, A. K. and Bishop, A. C.: An appinitic facies associated with certain granites in Jersey, Channel Islands, *J. Geol. Soc. Lond.*, 111, 143–166, <https://doi.org/10.1144/gsjgs.140.6.0921>, 1955.
- Whitney, D. L. and Evans, B. W.: Abbreviations for names of rock-forming minerals, *Am. Mineral.*, 95, 185–187, <https://doi.org/10.2138/am.2010.3371>, 2010.
- Wise, S. A. and Waters, R. L.: Certificate of Analysis. Standard Reference Material 987. Strontium Carbonate (Isotopic Standard), https://tsapps.nist.gov/srmext/certificates/archives/987_May1,2000.pdf (last access: 9 October 2023), 2007.
- Woodhead, J. D., Hergt, J. M., Davidson, J. P., and Eggins, S. M.: Hafnium isotope evidence for “conservative” element mobility during subduction zone processes, *Earth Planet. Sc. Lett.*, 192, 331–346, [https://doi.org/10.1016/S0012-821X\(01\)00453-8](https://doi.org/10.1016/S0012-821X(01)00453-8), 2001.
- Xiong, F., Ma, C., Wu, L., Jiang, H., and Liu, B.: Geochemistry, zircon U–Pb ages and Sr–Nd–Hf isotopes of an Ordovician appinitic pluton in the East Kunlun orogen: New evidence for Proto-Tethyan subduction, *J. Asian Earth Sci.*, 111, 681–697, <https://doi.org/10.1016/j.jseaes.2015.05.025>, 2015.
- Zhang, X., Xue, F., Yuan, L., Ma, Y., and Wilde, S. A.: Late Permian appinite–granite complex from northwestern Liaoning, North China Craton: Petrogenesis and tectonic implications, *Lithos*, 155, 201–217, <https://doi.org/10.1016/j.lithos.2012.09.002>, 2012.